Journal of Mammalian Evolution (2026) 33:6
https://doi.org/10.1007/s10914-025-09793-0

RESEARCH

New evidence from the bony labyrinth and teeth of the Late Miocene ape *Oreopithecus* based on a partial cranium from Baccinello

Alessandro Urciuoli[1,2,3,4] · Clément Zanolli[5] · Florian Bouchet[2] · Júlia Arias-Martorell[2] · Loïc Costeur[6] · Lorenzo Rook[7] · David M. Alba[2]

Received: 14 August 2025 / Accepted: 4 December 2025

Abstract

Oreopithecus bambolii, from the Tusco-Sardinian archipelago, is the latest-known European Miocene ape and a longstanding evolutionary enigma, owing to its mosaic morphology. Its systematic position has been intensely debated, resulting in a broad spectrum of hypotheses, ranging from a dryopithecine great ape to a nyanzapithecid stem hominoid, a giant hylobatid, or even a pliopithecoid. We reassess these competing hypotheses based on new data from the bony labyrinth and teeth of a partial cranium (Bac 62) from Baccinello (8.3–7.7 Ma). Diffeomorphic deformation analysis of the semicircular canals (SCs) and vestibule, dental tissue proportions, and enamel-dentine junction shape were used to compare *Oreopithecus* with a sample of extant and extinct anthropoids. Our results confirm that the SCs and vestibule of *Oreopithecus* combine some derived crown hominoid synapomorphies and crown hylobatid-like characters with the retention of anthropoid symplesiomorphies that preclude a straightforward classification. In turn, the enamel-dentine junction shape of the upper molars markedly differs from that of dryopithecines and extant hominoids but only shows some similarities with that of pliopithecoids, while the analysis of tooth tissue proportions reveals thick enamel. Our results, combined with previous evidence based on cranial morphology, strongly argue against a close phylogenetic relationship with Miocene apes from Europe and do not particularly support a close relationship with hylobatids. Instead, they are more consistent with *Oreopithecus* being a derived stem hominoid, although the scarce available data for nyanzapithecids precludes adequately testing this hypothesis and some similarities with pliopithecoids remain intriguing and deserve further investigation.

Keywords Enamel-dentine junction · Evolution · Geometric morphometrics · Hominoidea · Phylogeny · Semicircular canals

✉ Alessandro Urciuoli
alessandro.urciuoli@pim.uzh.ch

[1] Department of Paleontology, University of Zurich, Karl-Schmid-Strasse 4, Zurich 8006, Switzerland

[2] Institut Català de Paleontologia Miquel Crusafont (ICP-CERCA), Universitat Autònoma de Barcelona, Edifici ICTA-ICP, c/ Columnes s/n, Campus de la UAB, 08193 Cerdanyola del Vallès, Barcelona, Spain

[3] Division of Palaeoanthropology, Senckenberg Research Institute and Natural History Museum Frankfurt, Senckenberganlage 25, 60325 Frankfurt am Main, Germany

[4] Departamento de Ciencias de la Vida, Universidad de Alcalá, Cátedra de Otoacústica Evolutiva y Paleoantropología (HM Hospitales-UAH), Alcalá de Henares, Madrid 28871, Spain

[5] Univ. Bordeaux, CNRS, MCC, PACEA, UMR 5199, Pessac F-33600, France

[6] Natural History Museum Basel, Augustinergasse 2, Basel 4001, Switzerland

[7] Dipartimento di Scienze della Terra, Università degli Studi di Firenze, Firenze, Italy

Published online: 31 March 2026

Introduction

Oreopithecus in the framework of Miocene ape evolution

Within the complex picture of hominoid (ape and human) evolution, *Oreopithecus bambolii* Gervais, 1872a stands out as a particularly enigmatic taxon. Recorded from Late Miocene deposits of the Tusco-Sardinian Paleobioprovince—a paleoarchipelago encompassing parts of modern Tuscany and Sardinia in Italy—dated to ~ 8.3–6.7 Ma (Abbazzi et al. 2008; Casanovas-Vilar et al. 2011; Rook et al. 2011; Rook 2016), it represents the latest known non-cercopithecoid catarrhine from Europe. Furthermore, despite having been described more than 150 years ago (Gervais 1872a, b) and being one of the most completely preserved Miocene apes from Europe, a consensus has yet to be reached regarding its systematic position (see review in Alba et al. 2024).

The phylogenetic controversy about *Oreopithecus* stems from the contrasting evidence provided by different anatomical regions. The cranium appears more plesiomorphic than that of hominids (great apes and humans), showing many similarities with stem catarrhines (pliopithecoids), stem hominoids (particularly, nyanzapithecids), and hylobatids (Alba et al. 2024). Some previous authors recognized a few cranial synapomorphies of crown hominids in *Oreopithecus* (Andrews et al. 1996; Harrison and Rook 1997; Moyà-Solà and Köhler 1997; Alba et al. 2001b; Rook et al. 2004)—including Salvador Moyà-Solà, to whom this article is dedicated (see further details in the following subsection). However, the short and low face of *Oreopithecus*, coupled with its relatively small neurocranium, are more likely to represent the plesiomorphic condition for hominoids and even catarrhines (Harrison 1987, 1989; Jungers 1987; Begun and Kordos 2004; Alba 2010; Alba et al. 2015). The inner ear semicircular canals (SCs) and vestibule—encasing the organs for gaze stabilization and acceleration perception (see below for further anatomical details)—show some (but not all) crown hominoid synapomorphies and no crown-hominid synapomorphies other than the thick canals—probably independently acquired—otherwise retaining a more plesiomorphic condition (Urciuoli et al. 2020, 2021a, b). On the other hand, the dentition of *Oreopithecus* is highly distinctive and seemingly derived, superficially resembling in several features the occlusal pattern of cercopithecoids (Old World monkeys)—particularly regarding the nearly transverse arrangement of the molar cusps (Delson 1979; Szalay and Delson 1979; Harrison 1987; Harrison and Rook 1997). Several authors have noted more detailed dental similarities with nyanzapithecids from Africa (Harrison 1986, 1987, 1991; Rossie and Cote 2022; Alba et al. 2024), as supported by recent cladistic analyses (Nengo et al. 2017; Gilbert et al. 2020), which would imply their joint inclusion in a single family Oreopithecidae—as done by multiple authors over the years (Schwalbe 1915; Leakey 1967, 1968; Harrison, 1986, 1991; Benefit and McCrossin 2001; Pugh et al. 2025). However, a preliminary analysis of endostructural lower molar shape revealed similarities with pliopithecoids (Zanolli et al. 2022a), thereby supporting the similarities in occlusal morphology previously noted by Hill et al. (2013)—see discussion in Alba et al. (2024). Lastly, the postcranium of *Oreopithecus* exhibits orthograde traits that closely resemble those of crown hominoids and have been used to interpret this taxon as close to the hylobatid–hominid divergence or even as a stem hominid (Harrison 1987, 1991; Sarmiento 1987; Harrison and Rook 1997; Moyà-Solà et al. 1997). Given the contradictory evidence provided by the craniodental and postcranial evidence, it is currently considered that such crown-hominoid similarities are more likely the result of evolutionary convergence (i.e., homoplasies) rather than homologies reflecting common descent with crown hominoids (Pugh 2022; Almécija et al. 2021; Urciuoli and Alba 2023; Alba et al. 2024).

Salvador Moyà-Solà and the study of *Oreopithecus*

Given that this work belongs to a collection of papers in honor of Salvador Moyà-Solà, it is worth briefly reviewing the role played by him and his collaborators from the 1990s onward in the current understanding of *Oreopithecus* (see a review in Alba 2025). Moyà-Solà first inspected fossils of *Oreopithecus* when visiting the Naturhistorisches Museum Basel (Switzerland) in 1986, before extensively devoting himself to the study of fossil primates (Alba 2025). However, it was not until a decade later, after discovering a partial skeleton of the Miocene ape *Hispanopithecus* from Can Llobateres in Spain showing an orthograde body plan (Moyà-Solà and Köhler 1996), that he became seriously engaged in the study of *Oreopithecus*—which merged his two main research interests, namely Miocene apes and evolution under insularity conditions (Alba 2025). In collaboration with Meike Köhler, he first advanced the hypothesis that *Oreopithecus* represents an insular descendant of European dryopithecines (Moyà-Solà and Köhler 1997)—published in parallel to Harrison and Rook's (1997) book chapter that reached similar conclusions. This view not only implied a great ape status for *Oreopithecus* but further favored a European origin for this taxon, with Moyà-Solà and Köhler (1997) specifically advocating a pedomorphic hypothesis to explain differences in cranial morphology (see also Alba et al. 2001a, b). The same year, Köhler and Moyà-Solà (1997) revived the controversy about the locomotor repertoire of *Oreopithecus*, supporting a significant component of a unique form of terrestrial bipedalism that would

have evolved as a result of insularity-related selection pressures. Their views, further supported by some subsequent studies coauthored by Moyà-Solà (Rook et al. 1999), challenged the prevailing consensus that *Oreopithecus* was a primarily arboreal (climbing and suspensory) ape (Harrison 1987, 1991; Sarmiento 1987) and were not particularly well received (Alba 2025). Even more controversial was Moyà-Solà et al.'s (1999) proposal that the *Oreopithecus* hand had human-like proportions and was capable of precision grasping, which they interpreted as a result of being freed from locomotor demands (due to the adoption of bipedal locomotion) in an insular context (see also Moyà-Solà 2000; Moyà-Solà and Köhler 2000, 2003; Köhler and Moyà-Solà 2003). Finally, a pioneering study of the *Oreopithecus* inner ear bony labyrinth, in which Moyà-Solà participated as coauthor, supported its great ape status based on the SCs (Rook et al. 2004).

Most of the interpretations supported by Moyà-Solà and colleagues during the late 1990s and early 2000 s were controversial or, at least, not generally accepted (Alba 2025)—particularly regarding bipedalism (Russo and Shapiro 2013; Hammond et al. 2020) and precision grasping (Susman 2004, 2005; but see Moyà-Solà et al. 2005), but also in regards to its purported close phylogenetic relationships with dryopithecines and its great ape status overall (Nengo et al. 2017; Gilbert et al. 2020; Urciuoli and Alba, 2023; Alba et al. 2024). More recent analyses, in which Moyà-Solà participated, rather suggested that the manual proportions (Almécija et al. 2014), torso morphology (Hammond et al. 2020), and SCs (Urciuoli et al. 2020, 2021a, b) of *Oreopithecus* are plesiomorphic as compared with the hominid condition. The same probably applies to its cranial morphology (Alba et al. 2024), thereby supporting the view that *Oreopithecus* is probably a stem hominoid postcranially convergent with modern apes due to the independent acquisition of orthograde features (Pugh 2022; Urciuoli and Alba 2023; Alba et al. 2024). Yet, the work performed by Moyà-Solà and colleagues more than two decades ago played a pivotal role in reinvigorating the interest on *Oreopithecus* by placing it at the center of the debate and prompting further research. *Oreopithecus* epitomizes the challenge of postcranial homoplasy in hominoid phylogenetics and undoubtedly remains as a key taxon for disentangling the many uncertainties that still remain about the evolutionary history of apes (Urciuoli and Alba 2023; Alba et al. 2024). As noted by Alba et al. (2024), more confidently resolving the phylogenetic relationships of *Oreopithecus* offers the prospect of better clarifying those of hominoids as a whole, given the suspicion that postcranial homology between hylobatids and hominids might be causing a problem of long-branch attraction in cladistic analyses (Urciuoli and Alba 2023). Of particular interest are some dental similarities between *Oreopithecus* and pliopithecoids (Hill et al. 2013; Zanolli et al. 2022a; Alba et al. 2024), particularly in the light of the fact that some of the latter further independently acquired crown hominoid-like postcranial features (Alba et al. 2015; Bouchet et al. 2024b).

The inner ear bony labyrinth and teeth of *Oreopithecus*

All anatomical structures are potentially subject to homoplasy and, hence, susceptible to providing a misleading signal in phylogenetic inference. However, recent analyses have shown that structures that develop during early ontogenetic stages and do not undergo subsequent remodeling are a good source of phylogenetically informative characters (Skinner et al. 2008). This is the case of the inner ear bony labyrinth in mammals (Ekdale 2013). Composed of a set of fluid-filled cavities located within the petrous portion of the temporal bone, it houses the sensory organs of balance (the three semicircular ducts and otolith organs; Rabbitt 2019) and hearing (the cochlea; Heffner 2004), which are constituted of delicate, fluid filled membranes where the sensory epithelia are found. The bony labyrinth (Fig. 1) is composed of three—anterior (ASC), posterior (PSC), and lateral (LSC)—almost orthogonal SCs that are located posterolaterally, the vestibular recesses (anteromedially attached to the SCs), and the cochlea (found anteriomedially and connected to the vestibular recesses). The ASC and PSC merge before reaching the vestibule, forming a single canal termed common crus (CC). The spatial relationship between the bony labyrinth and the encased membranes varies among species (especially for the SCs and ducts; Ramprashad et al. 1986) and is the focus of ongoing research (Smith et al. 2023; Hussain et al. 2023). Furthermore, despite the close spatial and ontogenetic relationship of the organs encased by the bony labyrinth, its shape (especially that of the SCs) embeds a strong phylogenetic signal (Morimoto et al. 2020; Urciuoli et al. 2020, 2021a, b; del Río et al. 2021; Zhang et al. 2024). Previous analyses showed that several features of the SCs are pertinent to the phylogenetic debate about *Oreopithecus*. In particular, this taxon shows a large vestibule, and thick and small (particularly the LSC) SCs, more similar to those of extant hominids than to the larger, slenderer SCs of platyrrhines, stem catarrhines, cercopithecoids, and hylobatids, which likely retain the plesiomorphic anthropoid condition (Rook et al. 2004; Urciuoli et al. 2021b). *Oreopithecus* also displays several bony labyrinth synapomorphies of crown hominoids—a vertically compressed anterior canal and short common crus (CC)—coupled with an additional similarity (an anterosuperiorly projecting anterior canal) specifically with extant hylobatids and orangutans (Urciuoli et al. 2020, 2021a, b). This mosaic morphology of *Oreopithecus*

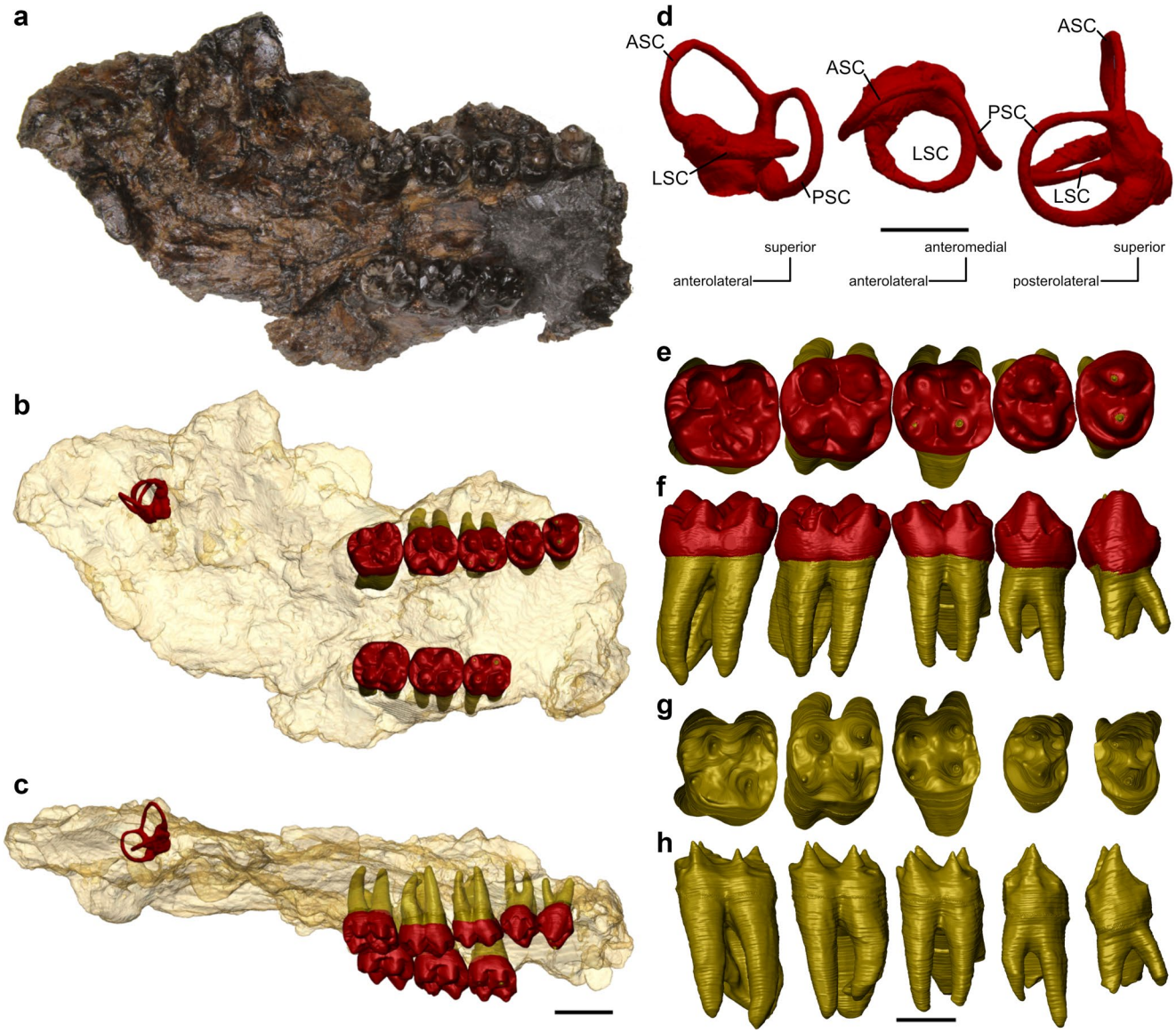

Fig. 1 **a**–**c**. Photograph (**a**) and virtual renderings (**b**–**c**) of the partial cranium of *Oreopithecus bambolii* Bac 62, in inferior (**a**–**b**) and right lateral (**c**) views. The bone in panels **b**–**c** is semitransparent, showing the SCs, the vestibule, and the teeth. **d.** right semicircular canals and vestibule in posterolateral (left), superolateral (middle), and posteromedial (right) views; **e**–**h.** right cheek teeth in occlusal (**e**, **g**) and buccal (**f**, **h**) views, medial to right, displaying the external morphology (red; **e**–**f**), and EDJ (yellow; **g**–**h**). The segmented teeth in **e**-**h** were isolated and reoriented to account for specimen deformation. Abbreviations: **ASC**, Anterior semicircular canal; **LSC**, Lateral semicircular canal; **PSC**, Posterior semicircular canal. Scale bars equal 1 cm (**a**–**c**) and 5 mm (**d**–**h**)

cannot be easily reconciled with any of the competing phylogenetic hypotheses mentioned above without assuming some degree of homoplasy (convergence and/or reversal). In particular, the LSC of *Oreopithecus* lacks the marked superiorly bending of the ampullary portion found in crown hominoids, supporting the stem hominoid status of the former, even if its vertically compressed anterior canal and short CC are potentially synapomorphic with crown hominoids (Urciuoli et al. 2021a). However, if *Oreopithecus* is a stem hominoid, the large vestibule and stout SCs of this taxon must be interpreted as convergences with hominids, or else as crown-hominoid synapomorphies subsequently reversed in hylobatids (Urciuoli et al. 2021a). It is, however, noteworthy that fossil evidence for the bony labyrinth is often meager (in the case of *Oreopithecus*, a single specimen had been analyzed so far), which hinders a proper evaluation of intraspecific variation, potentially biasing the results.

Another anatomical structure that is formed during early ontogenetic stages (both prenatally and soon after birth) is the enamel-dentine junction (EDJ) of molars (particularly, the first and second molars). The EDJ is a highly genetically

constrained structure, whose shape is regarded as highly informative from a taxonomic viewpoint and useful to distinguish among extinct and extant primate taxa (Skinner et al. 2008; Pan et al. 2020; Zanolli et al. 2022a, 2023; Bouchet et al. 2024a). The EDJ shape also holds a strong phylogenetic signal that can be analyzed to reconstruct evolutionary relationships among catarrhines using geometric morphometrics (Zanolli et al. 2022b). At the level of the outer enamel surface, the lower molars of *Oreopithecus* display similarities with those of nyanzapithecids (Rossie and Cote 2022), but the presence of multiple secondary cusps and crests makes the recognition of homologies subject to interpretation (see discussion in Alba et al. 2024), with some crests topologically resembling the mesial and distal arms of the pliopithecine triangle characteristic of pliopithecoids (Hill et al. 2013). Given the taxonomic and phylogenetic significance of the EDJ, preliminary analyses of the lower molar EDJ shape of *Oreopithecus* were conducted by Zanolli et al. (2022a). The results showed that the lower molars of *Oreopithecus* differ from those of extant great apes, dryopithecines, and two nyanzapithecid specimens (which are rather dryopithecine-like), and more closely resemble the pliopithecoid pattern. Similar analyses, however, have yet to be conducted based on the upper molar EDJ shape. Such studies are currently ongoing, and the teeth here reported will be included in future 3DGM analyses based on additional material available for *Oreopithecus*.

Aims of this study

To further evaluate the phylogenetic relationships of *Oreopithecus* based on the two aforementioned anatomical structures, here we rely on an unpublished, crushed and partial cranium (Bac 62) of *O. bambolii*, for which only M2 dental wear had been previously assessed (Galbany et al. 2006). Using microcomputed tomography (μCT) techniques, we describe in detail the SCs and vestibule, as well as the upper cheek teeth, and compare them with those of extant and other extinct anthropoids, both qualitatively and quantitatively using morphometric analyses. Based on these comparisons, we assess the plausibility of various competing phylogenetic hypotheses for *Oreopithecus*—namely, the pliopithecoid (stem catarrhine), the nyanzapithecid (stem hominoid), and the stem hylobatid hypotheses.

Materials and methods

Studied specimen

The studied specimen is a partial and crushed cranium (Bac 62) of *O. bambolii* housed in the collection of the Naturhistorisches Museum Basel, Switzerland. It was recovered from the coal mines of Baccinello (Tuscany, Italy) by Johannes Hürzeler during the 1950–1960s (Hürzeler 1958; Engesser 2000). No precise location of the finding is recorded but it is considered to be roughly coeval with other *Oreopithecus* remains from the V1 faunal assemblage, which is dated to 8.3–7.7 Ma (Rook 2016) and further yielded the specimen Bac 183 (an *Oreopithecus* petrosal bone μCT scanned and described in Rook et al. 2004). The μCT scan of Bac 62 was performed at the Department of Paleontology of the University of Zurich, Switzerland, using an XT H 225 ST Nikon Metrology microtomographic scanner with the following scanning parameters: voltage = 121 kV, current = 197 μA, and no filter. The resulting isometric voxel size was 57.8 μm. Due to preservation, only the left vestibular system bony labyrinth could be segmented in Avizo 9.0.1 software (FEI Visualization Sciences Group). Most of the upper postcanine dentition is preserved, including the two left premolars and all the upper molars. All dental elements were segmented in Avizo, although due to the lack of comparative data, morphological comparisons of the EDJ are limited to the upper molars. The 3D models of the vestibular system bony labyrinth, as well as those of the outer enamel surface and enamel/dentine junction of the upper molars are available from MorphoSource (www.morphosource.org).

Inner ear bony labyrinth

Comparative sample for the bony labyrinth

The comparative sample for the three-dimensional geometric morphometric (3DGM) analyses of the SCs and vestibule was selected to provide a broad phylogenetic context for interpreting the shape of *Oreopithecus*. The extant anthropoid sample comprised the μCT scans of 230 crania and temporal bones belonging to 36 species and 31 genera of anthropoid primates, including a wide selection of platyrrhines, cercopithecoids, and all extant hominoid genera (Online Resource 1: Table S1). We also analyzed 22 fossil specimens belonging to 15 extinct anthropoid species (Online Resource 1: Table S2) to adequately assess the phylogenetic affinities of Bac 62. These comprised another individual of *O. bambolii* (previously, erroneously reported as Bac 208; Rook et al. 2004; Urciuoli et al. 2020, 2021a, b), the stem anthropoid *Parapithecus grangeri* (Bush et al. 2004); the stem platyrrhines *Dolichocebus gaimanensis* (Kay et al. 2008), *Homunculus patagonicus* (Fulwood et al. 2016), and *Tremacebus harringtoni* (Fulwood et al. 2016); the early stem catarrhines *Aegyptopithecus zeuxis* (Simons et al. 2007), *Saadanius hijazensis* (Zalmout et al. 2010, 2020), *Epipliopithecus vindobonensis* (Urciuoli et al. 2021a), and *Pliobates cataloniae* (Urciuoli et al. 2022a), the

two last species included in the Pliopithecoidea (Bouchet et al. 2024b); the stem cercopithecoid *Victoriapithecus macinnesi* (Urciuoli et al. 2022a); the stem hominoids *Ekembo heseloni* (Urciuoli et al. 2022a) and *Nacholapithecus kerioi* (Kunimatsu et al. 2019); the stem hominids *Hispanopithecus laietanus* (Urciuoli et al. 2021b) and *Rudapithecus hungaricus* (Urciuoli et al. 2021b); and the hominins *Australopithecus africanus* (Beaudet 2019) and *Homo erectus* (Urciuoli et al. 2022b). The scans were accessed through different sources listed in Online Resource 1: Table S2.

Shape analysis of the bony labyrinth

The shape of the SCs and vestibule was analyzed using a landmark-free, deformation-based 3DGM technique termed diffeomorphic deformation analysis (DDA; Beaudet 2025), also known as diffeomorphic surface matching (e.g., Durmoncel et al. 2014; Beaudet et al. 2016; Zanolli et al. 2023). This approach does not rely on geometrical landmarks but instead examines the geometrical correspondence between continuous surfaces (Durrleman et al. 2012a; Bône et al. 2018). The method relies on the computational construction of a sample-average surface model (a template) and then quantifies the deformation required to match this template to each individual target surface in the analysis (Glaunès and Joshi 2006; Durrleman et al. 2012a, b). Prior to the analysis, the unscaled 3D surfaces were aligned using the 'Align Surface' module of Avizo v. 9.0.1 (FEI Visualization Sciences Group, Houston), which minimizes the distances between the faces of each surface through rigid translation, rotation, and uniform scaling (Urciuoli et al. 2021b).

The transformations between surfaces are mathematically modeled as diffeomorphisms—one-to-one deformations of the 3D space that are smooth, invertible, and have a smooth inverse (Durrleman et al. 2012a). The final output of this process is a set of high-dimensional vectors, or 'momenta,' which represent the flow of deformations from the control points on the template to the target shape, thus describing both the direction and magnitude of shape change (Bône et al. 2018). Due to the high computational power required for these analyses, the diffeomorphisms and momenta were computed using the open-source software Deformetrica v. 4.3 (Bône et al. 2018) on the high-performance computing cluster DeepFry (LOEWE Centre for Translational Biodiversity Genomics, Frankfurt am Main, Germany).

Statistical analysis of the bony labyrinth shape data

The sets of vectors (momenta) generated by the deformation analysis were used as shape variables for subsequent statistical analyses. The data were analyzed in Rstudio v. 2023.9.0.463 (RStudio Team 2023) for R v. 4.3.1 (R Core Team 2023) using the RToolsForDeformetrica v. 0.1 package (Dumoncel 2021). Major patterns of interspecific shape variation were explored using a between-group principal components analysis (bgPCA) performed on the deformation fields (the raw shape data) with the '*groupPCA'* function of the Morpho v. 2.8 package for R (Schlager 2017), considering major clades (i.e., platyrrhines, cercopithecoids, hylobatids, and hominids) as a priori grouping factors. Fossil specimens, including Bac 62, were projected a posteriori onto the resulting morphospace to assess their affinities without influencing the main axes of variation. The morphological affinities of fossil specimens to the extant groups were further quantified by computing typicality probabilities of group membership using the '*typprob'* function of Morpho package for R (Schlager 2017). An interactive HTML 3D plot of the first three bgPCs was generated using the R package plotly v. 4.10.4 (Sievert et al. 2021). The extreme conformation shape for the bgPCs was obtained by rotating the bgPC scores back into the raw shape space to obtain the corresponding set of momenta. These were then used to perform a "shooting" (i.e., an iterative deformation of the sample mean toward the targeted momenta) using the 'compute' function of Deformetrica. The deformations from the sample mean were rendered by means of a continuous pseudocolor scale obtained using the 'add_colormap_shooting' python script (Dumoncel 2021). We also computed local maximal displacements using the 'add_local_maximal_momenta_shooting' python script (Dumoncel 2021) and visualized them as vectors (indicating magnitude and amount of deformation) in Paraview 5.6.0 (Kitware).

To ensure that the observed grouping structure was not spurious, the bgPCA results were compared to those obtained using a cv-bgPCA (Cardini and Polly 2020). The group mean differences were assessed using a permutational analysis of variance (PERMANOVA, with 1000 permutations) performed on the Euclidean distances between the means. We also used the vegan v. 2.5 package (Oksanen et al. 2019) in R to compute *Z*-scores and determination coefficients (R^2, denoting the amount of variance accounted by group differences) for the raw shape data and the bgPCA scores, both standard and cross-validated (Cardini and Polly 2020).

Phylomorphospace and phylogenetic trees

To visualize the direction and magnitude of morphological evolution, we employed a phylomorphospace approach (Sidlauskas 2008). This method involves projecting a phylogenetic tree onto the morphospace derived from the bgPCA performed on the DDA shape data. The positions of the internal nodes, representing the last common ancestors (LCAs), were estimated using a maximum-likelihood method implemented via the *'fastAnc'* function in the phytools v. 0.6e60 package for R

(Revell 2012). The tips of the tree branches correspond to the centroid scores for each genus, whereas branch lengths reflect the phylogenetic relationship among the considered genera and time-distances from the ancestral nodes.

To consider the debate about the systematic position of *Oreopithecus*, we repeated the analyses using three alternative cladogram topologies, each one reflecting one of the main phylogenetic hypotheses previously advocated for this taxon (Online Resource 1: Fig. S3), namely: a pliopithecoid (stem catarrhine), a stem hylobatid, or a nyanzapithecid (stem hominoid). The phylogeny for extant taxa was based on the comprehensive molecular data from Kuderna et al. (2023), with the divergence age for *Symphalangus syndactylus* specifically informed by Shao et al. (2023). Extinct species were subsequently integrated into this tree based on their phylogenetic position as inferred from previously performed cladistic analyses (Seiffert 2012; Kay 2015; Fulwood et al. 2016; Nengo et al. 2017; Gilbert et al. 2020) and corresponding to the three aforementioned hypotheses (Online Resource 1: Fig. S3). Their divergence was arbitrarily set to 1 Myr prior to the next successive node and their tip ages defined by their currently accepted chronostratigraphic age. To create visual representations of the ancestral morphologies, the estimated bgPC scores for each LCA were rotated and translated back from the morphospace into the deformation field space using the RToolsForDeformetrica package for R. This process generated a set of momentum vectors, which were then used in Deformetrica to warp the sample template surface into the predicted 3D shape of the target LCA. The shape distance between *Oreopithecus* and the selected estimated LCAs (namely, the crown hominoid, crown hylobatid, and pliopithecoid LCAs) was eventually quantified by calculating the Euclidean distances between the LCA bgPC scores and the *Oreopithecus* centroid using the *'dist'* function from the base stats package in R.

Teeth

Description and measurements of occlusal shape

Dental measurements of mesiodistal length (MD) and buccolingual breadth (BL) were digitally taken from the outer enamel surface (OES) models to the nearest 0.1 mm. For the molars, BL was measured separately at the mesial (BLm) and distal (BLd) lobes. To quantify crown proportions, a breadth/length index was computed (in percentage) as BLI = maximum BL/MD × 100. The descriptions of the OES were based on the fossil specimen with the aid of surface models, whereas the EDJ shape of the molars was compared with that of other Miocene hominoids and pliopithecoids available from the literature (Fortuny et al. 2021; Bouchet et al. 2024a). The tooth tissues (enamel, dentine, and pulp) were segmented in Avizo using a semi-automatic, threshold-based method. The volumes of the dental tissues were computed using the same software.

Tooth tissue proportions

The 3D tooth tissue proportions of the upper molars of Bac 62 were compared with those of other Miocene and extant non-cercopithecoid catarrhines. We followed Olejniczak et al. (2008) to cut the crown along the cervical plane, taking the mid-plane between the plane showing the last points of enamel and that showing a complete enamel ring. Following measurements of enamel volume (V_e, in mm^3), crown dentine and pulp volume (V_{cdp}, in mm^3) and surface area of the enamel-dentine junction (S_{EDJ}, in mm^2), we computed three indices. Three-dimensional average enamel thickness (3DAET; in mm) and three-dimensional relative enamel thickness (3DRET; dimensionless) were computed as follows (Olejniczak et al. 2008): $3DAET = V_e/S_{EDJ}$ and $3DRET = 3DAET \times 100/V_{cdp}^{1/3}$. Given that 3DAET is a metrical variable (and, thus, correlated with tooth size), it is not suitable to compare species of different size. 3DRET, in contrast, is standardized by the cube root of V_{cdp} and, hence, a dimensionless shape index, more suitable for comparisons among taxa (Olejniczak et al. 2008). The recently developed ratio of enamel-thickness to dentine-thickness (3DRED; dimensionless) was also computed based on the following formula (Yi et al. 2021): $3DRED = 10 \times (3DAET/(V_{cdp}/S_{EDJ}))^{1/3} = 10 \times (V_e/V_{cdp})^{1/3}$. The latter index is less sensitive to differences in scanning parameters (especially in voxel size disparity) and, like 3D RET, represents an additional size-standardized variable to assess the taxonomic value of enamel thickness in primate teeth (Yi et al. 2021). We compared the tissue proportions of Bac 62 upper molars with those of *Pierolapithecus catalaunicus*, *Anoiapithecus brevirostris*, *Dryopithecus fontani*, *Hispanopithecus crusafonti*, *Hispanopithecus laietanus*, *Pongo pygmaeus*, *Pan troglodytes*, *Gorilla gorilla*, *Hylobates muelleri* and *Hylobates* sp., and *Symphalangus syndactylus* (Olejniczak et al. 2008; Zanolli et al. 2019; Fortuny et al. 2021; Sineo et al. 2024).

Abbreviations: 3DAET, Three-dimensional average enamel thickness; **3DGM**, three-dimensional geometric morphometrics; **3DRED**, ratio of enamel-thickness to dentine-thickness; **3DRET**, three-dimensional relative enamel thickness; **AMNH**, American Museum of Natural History, New York, USA; **ASC**, anterior semicircular canal; **Bac**, Baccinello collection at the Naturhistorisches Museum Basel, Switzerland; **bgPC**, between-group principal component; **bgPCA**, between-group principal component analysis; **BL**, maximum buccolingual breadth; **BLI**, breadth/length index; **BLm**, BL at the mesial lobe; **BLd**, BL at the distal lobe; **CC**, common crus; **cv-bgPCA**, cross-validated

bgPCA; **DDA**, diffeomorphic deformations analysis; **EDJ**, enamel-dentine junction; **IPS**, acronym of the collections of the Institut Català de Paleontologia Miquel Crusafont (formerly, Institut de Paleontologia de Sabadell), Barcelona, Spain; **LCA**, last common ancestor; **LSC**, lateral semicircular canal; **MCZ**, Museum of Comparative Zoology, Harvard University, Cambridge, USA; **MD**, mesiodistal length; **MFN**, Museum für Naturkunde Berlin, Germany; **MGSB**, Museu Geològic del Seminari Conciliar de Barcelona, Spain; **MGUP TOS**, Museo di Geologia Gemmellaro Università di Palermo, Italy; **µCT**, microcomputed tomography; **MSNT**, Museo di Storia Naturale of Trieste; **PERMANOVA**, permutational analysis of variance; **PSC**, posterior semicircular canal; **SCs**, semicircular canals; SS_{EDJ}, surface area of the enamel-dentine junction; V_{cdp}, crown dentine and pulp volume; V_e, enamel volume

Results

Description and preservation

The partial cranium Bac 62 (Fig. 1), like most *Oreopithecus* specimens, is heavily crushed (in this case, in superoinferior direction) due to diagenetic processes. These caused the collapse of the braincase, as well as the breakage of most cranial bones. Nonetheless, the cranium is fairly complete, missing only the rostral-most portion of the premaxilla (corresponding to the alveoli of the incisors, which are also missing), the zygomatic arches, and most of the occipital and the left temporal bone. In superior view, most of the bones are almost completely shattered, although fragments of the frontals, parietals, and (some) of the occipital are visible. In inferior view, the specimen appears much better preserved and cranial bones are clearly identifiable and unaffected by plastic deformation. Particularly, the palate is almost complete and fairly well-preserved (although a fracture between the palatine bones and the maxillae caused a slight detachment and anti-clockwise rotation of the former), Most of the cheek teeth are preserved except for the right premolars. They are only slightly worn, with very restricted dentine exposure at the apex of the premolar and some molar main cusps. The canines are missing but the left alveolus is relatively well preserved (albeit with a few fractures), whereas the right one is almost completely crushed. The left canine alveolus displays a round cross section and is small (MD = 6.4 mm; BL = 5.6 mm) compared with the cheek teeth, overall suggesting that the partial cranium Bac 62 likely belongs to a female individual (Alba et al. 2001a). The sphenoid is also present, although both pterygoid processes and the alisphenoid are heavily damaged. Although most of the occipital bone (the entire left side) is missing, the right condyle and the pars basilaris are well preserved.

On the right side, the temporal bone preserves the basal part of the temporal process and the mandibular fossa, as well as the tubular ectotympanic (complete and protruding laterally) and the mastoid process (displaced and rotated medially due to the crushing). The oval and jugular foramina are also clearly visible and well preserved, whereas the carotid canal is missing due to extensive breakage of the anterior-most portion of the petrous part of the temporal. Internally, the bony labyrinth is poorly preserved, due to the collapse of most of the cochlear bony encasing. Similarly, no ossicles could be identified in the middle ear cavity, which was also crushed. However, the SCs and the vestibule (encapsulating the vestibular system ducts and otolith organs) are fairly well-preserved, with only part of the ASC broken and displaced relative to the rest of the canal, although we could place it back to its original position (Fig. 1 d).

Bony labyrinth morphology

Semicircular canal and vestibule shape

The SCs of Bac 62 (Fig. 1 d) show clear morphological similarities with the SCs of the previously described specimen Bac 183 (Rook et al. 2004). Particularly, the ASC is moderately large in its curvature radius and shows a marked anterosuperior projection in its anterior-most portion (as in Bac 183, hylobatids, and *Pongo*). The ASC also shows a marked vertical compression, as in crown hominoids except *Homo*, and more marked than in the stem hominoid *Ekembo*. The PSC is round, as in most crown catarrhines, and roughly of the same curvature radius as the ASC and the LSC, differently from in the condition of Bac 183, where the LSC is smaller than the vertical canals. The LSC is also flat, like that of all non-hominoid anthropoids, and fairly round. The CC is very short (as in crown hominoids and *Ekembo*) and thick (as in crown and stem hominids). Unlike in Bac 183, only the CC is markedly thick, whereas the SCs appear moderately slender, showing an intermediate condition between those of hylobatids and hominids.

Diffeomorphic deformation analysis of the semicircular canals

We performed a bgPCA on the deformation fields obtained from the DDA to better assess the morphological affinities of Bac 62 relative to the comparative sample. The obtained bgPCs show a good separation among the four distinguished groups (i.e., platyrrhines, cercopithecoids, hominids, and hylobatids), with only a few areas of moderate overlap on intermediate bgPC1 to bgPC3 scores (Fig. 2; Online Resource 2). This is confirmed by the high classification accuracy of the bgPCA (97.4% of correctly classified

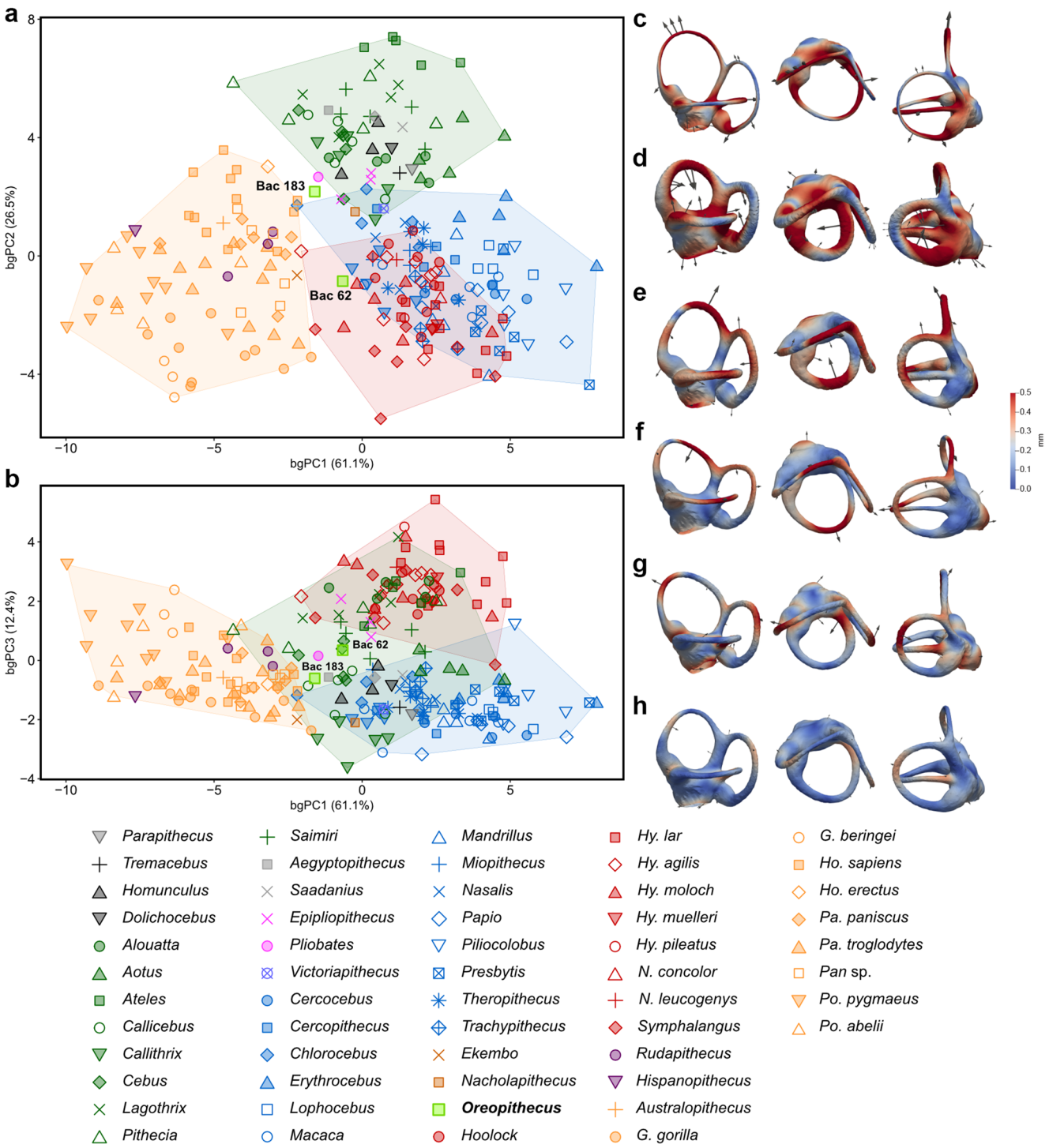

Fig. 2 **a**–**b**. Bivariate scatter plots of the bgPCA performed on the deformation fields (raw shape data) obtained from the diffeomorphic deformation analysis of the SCs and vestibule: bgPC2 vs. bgPC1 (**a**); bgPC3 vs. bgPC1 (**b**). The variance explained by each axis is given within parentheses. Symbols are colored based on taxonomic groups: stem anthropoids, dark gray; stem platyrrhines, black; crown platyrrhines, dark green; early stem catarrhines, light gray; pliopithecoids, fuchsia; stem cercopithecoids, navy blue; crown cercopithecoids, dark blue; stem hominoids, dark orange; hylobatids, red; dryopithecines, purple; crown hominids, light orange. A 3D interactive HTML plot of bgPC1 to bgPC3 using the same color coding can be found in Online Resource 2. **c**–**h.** Not-to-scale renders of 3D models showing the extreme conformations of shape variation for the axes shown in the bivariate plots (from left to right, in posterolateral, superolateral, and posteromedial views): bgPC1 maximum (**c**) and minimum (**d**); bgPC2 maximum (**e**) and minimum (**f**); bgPC3 maximum (**g**) and minimum (**h**). The 3D models are colored following a color gradient from blue (no displacement) to red (1.5 mm)

Table 1 Confusion matrix showing the classification results (percentages are within parentheses) obtained from the bgPCA performed on the SC shape data using major clades (platyrrhines, cercopithecoids, hominids, and hylobatids) as the grouping factor and based on typicality probabilities of group membership. Cross-validated classification results are shown in Online Resource 1: Table S3

A priori group	Classification			
	Cercopithecoids	Hominids	Hylobatids	Platyrrhines
Cercopithecoids	73 (97.4%)	1 (1.3%)	0 (0%)	1 (1.3%)
Hominids	0 (0%)	63 (98.4%)	0 (0%)	1 (1.6%)
Hylobatids	1 (2.1%)	1 (2.1%)	45 (95.8%)	0 (0%)
Platyrrhines	1 (2.2%)	0 (0%)	0 (0%)	44 (97.8%)

individuals), which only misclassified a few individuals (classification error $\leq$ 2.5% for any of the groups; Table 1). The high accuracy is kept even after cross-validation (96.1% of correctly classified individuals; Online Resource 1: Table S3). Indeed, the inspection of the scatterplot of the cross-validated bgPC scores (Online Resource 1: Fig. S1) shows minimal differences relative to those obtained with standard bgPCA. This is further confirmed by the *Z*-scores and R^2, which were computed to assess the presence of a grouping structure in the raw shape data ($Z = 9.744$; $R^2 = 0.306$), bgPCA scores ($Z = 15.597$; $R^2 = 0.699$), and cv-bgPCA scores ($Z = 15.869$; $R^2 = 0.712$). They show that, even if the correlation between the a priori grouping factor and the bgPC scores is higher than that with the raw shape data, the correlation is almost identical when cross-validated and standard bgPC scores are considered, thus allowing us to reject that grouping structure is spurious.

Along bgPC1 (61.1% of variance; Fig. 2a–d), crown hominids, dryopithecines, and the stem hominoid *Ekembo* (negative scores) are separated from most anthropoids (positive scores) except for a few platyrrhines and one individual of *Hylobates agilis* due to the possession of remarkably thick SCs and CC. Negative bgPC1 scores are further indicative of fairly small SCs relative to the whole vestibular system, as well as a less round and more laterally elongate PSC. The length of the CC and the position of the LSC relative to the PSC are also major drivers of bgPC1, so that species possessing a shorter CC and well-separated LSC and PSC planes (such as hominids) fall on negative scores. This also explains the moderately positive scores of hylobatids, which share with hominids a very short CC and separated LSC and PSC, yet combined with much thinner SCs and greater SC radii. The two *Oreopithecus* individuals slightly differ from one another along bgPC1 due to the presence of somewhat slenderer SCs in Bac 62 than in Bac 183. The bgPC2 (26.5% of variance; Fig. 2a, e–f) is mostly driven by differences in SC shape and relative size. This axis allows us to discriminate platyrrhines (extant and extinct), *Parapithecus*, and stem catarrhines (on markedly positive scores) from other anthropoids, albeit with some overlap. This is due to the presence in the former of markedly superiorly elongated ASC and PSC (only the PSC in the case of *Epipliopithecus* and *Pliobates*), as well as a long CC (Fig. 2e–f). *Homo* and the stem hominoid *Nacholapithecus* also fall on moderately positive bgPC2 scores due to the presence of large ASC and PSC relative to the smaller LSC. *Oreopithecus* appears quite variable in these features, as highlighted by the difference in bgPC2 scores between Bac 183 (positive and close to the range of *Homo* and platyrrhines) and Bac 62 (moderately negative), which is mainly caused by the larger LSC of the latter specimen. Hylobatids fall on positive scores for the bgPC3 (12.4% of variance; Fig. 2b, g–h), and are somewhat separated from most other anthropoids, except for a few *Pongo* and atelid individuals, which also fall on moderate positive scores. This is caused by the presence of an anterosuperior projection of the ASC anterior-most portion in both hylobatids and *Pongo*, whereas atelids share with hylobatids the possession of a mediolaterally compressed PSC. All these taxa also show a clear separation between the PSC plane and the LSC (Fig. 2g–h). Among fossils, only *Epipliopithecus* overlaps with the range of hylobatids (mainly due to the possession of a very separated LSC from the PSC plane), although Bac 62 somewhat approaches the hylobatid range of variation as a consequence of the moderately anterosuperiorly projecting anterior portion of the ASC.

When the three bgPCs are simultaneously considered (Online Resource 2), the two *Oreopithecus* individuals fall outside the convex hulls of all the considered groups, in a portion of the morphospace that is devoid of other specimens. This is reflected in the typicality probabilities based on the bgPC scores (Table 2). They show that Bac 62 represents an outlier for platyrrhines ($p < 0.05$) but not for all the remaining groups (with slightly greater affinities with cercopithecoids). Conversely, the bgPC scores of Bac 183 fit best with the distribution of platyrrhines and represents an outlier for both hylobatids and cercopithecoids. In turn, the analyzed stem anthropoid and stem catarrhines show greatest affinities and fall within the variation range of extant platyrrhines; stem hominoids and stem hominids match the variation of extant hominids and show greatest affinities with them (except for *Nacholapithecus*, which shows greater affinities with cercopithecoids); finally, the only analyzed stem cercopithecoid (*Victoriapithecus macinnesi*) shows clear affinities with extant cercopithecoids, although it does not represent an outlier for extant platyrrhines either.

Table 2 Typicality probability of group membership based on the bgPCA scores of selected fossil specimens. Non-significant probabilities ($p > 0.05$), implying that the individual does not represent an outlier for the distribution of the group bgPC scores, are in bold

Species	Catalog No.	Cercopithecoids	Hominids	Hylobatids	Platyrrhines
Oreopithecus bambolii	Bac 62	**0.096**	0.075	0.081	0.006
Oreopithecus bambolii	Bac183	0.048	0.050	<0.001	**0.246**
Parapithecus grangeri	CGM85785	0.002	<0.001	<0.001	**0.623**
Aegyptopithecus zeuxis	DPC18651	0.138	<0.001	<0.001	**0.207**
Aegyptopithecus zeuxis	DPC12081	0.009	<0.001	<0.001	**0.801**
Tremacebus harringtoni	FMI619	0.167	<0.001	<0.001	**0.278**
Dolichocebus gaimaensis	MACN-14128	0.058	<0.001	<0.001	**0.698**
Homunculus patagonicus	MP-MPV-3501	0.051	<0.001	<0.001	**0.612**
Homunculus patagonicus	MP-MPV-3502	0.012	<0.001	<0.001	**0.940**
Homunculus patagonicus	MP-MPV-3503	0.066	0.006	<0.001	**0.283**
Epipliopithecus vindobonensis	NHMW-1970/1397/0003	0.003	0.003	0.079	**0.092**
Epipliopithecus vindobonensis	NMB-OE-303 L	0.023	0.001	0.019	**0.455**
Epipliopithecus vindobonensis	NMB-OE-303 R	0.041	0.001	0.005	**0.683**
Pliobates cataloniae	IPS58443	0.024	0.025	0.001	**0.464**
Victoriapithecus macinnesi	KNM-MB-29100	**0.391**	0.002	<0.001	0.133
Ekembo heseloni	KNM-RU-2036al	0.049	**0.231**	<0.001	0.001
Nacholapithecus kerioi	KNM-BG-42744	**0.191**	0.007	<0.001	0.052
Hispanopithecus laietanus	IPS18000	<0.001	**0.352**	<0.001	<0.001
Rudapithecus hungaricus	RUD200	<0.001	**0.836**	0.001	<0.001
Rudapithecus hungaricus	RUD77L	0.007	**0.523**	0.003	0.010
Rudapithecus hungaricus	RUD77R	0.013	**0.475**	0.001	0.022

Phylomorphospace of the semicircular canals

The phylogenetic trees corresponding to the alternative phylogenetic hypotheses evaluated in this work for *Oreopithecus* were projected onto the morphospace by means of a phylomorphospace approach (Fig. 3). Overall, the bgPCA scores of the LCAs were minimally affected by the different tree topologies, with the only exception of the estimated LCA of crown hylobatids (Fig. 3d–e; Online Resource 1: Fig. S2d–f). Not surprisingly, when *Oreopithecus* is considered as a stem hylobatid, the shape configuration estimated for the crown hylobatid LCA appears less derived and more dissimilar from that of extant hylobatids (the anterior portion of the ASC does not project anterosuperiorly). Under the other two phylogenetic hypotheses (namely, the stem hominoid and pliopithecoid stem catarrhine ones), the hylobatid LCA shows a LSC that is well separated from the plane of the PSC and a moderately anterosuperiorly projecting anterior portion of the ASC. Overall, this LCA also shares clear similarities with cercopithecoids, due to the presence of slender and large SCs. The ancestral morphology for crown hominoids (Fig. 3c; Online Resource 1: Fig. S2a–c) is reconstructed as showing similarly-sized, round SCs, a fairly short CC, and moderately thick SCs (being closest to the morphology shown by *Ekembo*, although without the vertically compressed ASC of the latter). The absence of older and more basal pliopithecoids in the analysis is problematic for node calibration and, thus, the LCA reconstructed for this group should be interpreted with caution. Based on available data, their inferred ancestral shape is intermediate between that of platyrrhines, the stem cercopithecoid *Victoriapithecus*, and the stem hominoid *Nacholapithecus* (although closer to *Victoriapithecus* and cercopithecoids), showing a long CC, vertically elongate ASC and PSC, and a small LSC relative to the other SC (Fig. 3; Online Resource 1: Fig. S2g–i).

The similarity of *Oreopithecus* with the LCAs reconstructed for the aforementioned groups was assessed by means of Euclidean distances based on bgPCA scores (Table 3). These show a closest similarity (i.e., a shortest distance) between the *Oreopithecus* average and the crown hominoid LCA (independently of the phylogenetic hypothesis considered), whereas the pliopithecoid LCA and, even more so, the crown hylobatid LCA are markedly less similar. Closer similarities with the crown hominoid LCA are also found when the distances are computed separately for the two *Oreopithecus* individuals (Table 3), although similarities are less marked and Bac 62 (unlike Bac 183 and the *Oreopithecus* average value) is more similar to hylobatids than to pliopithecoids.

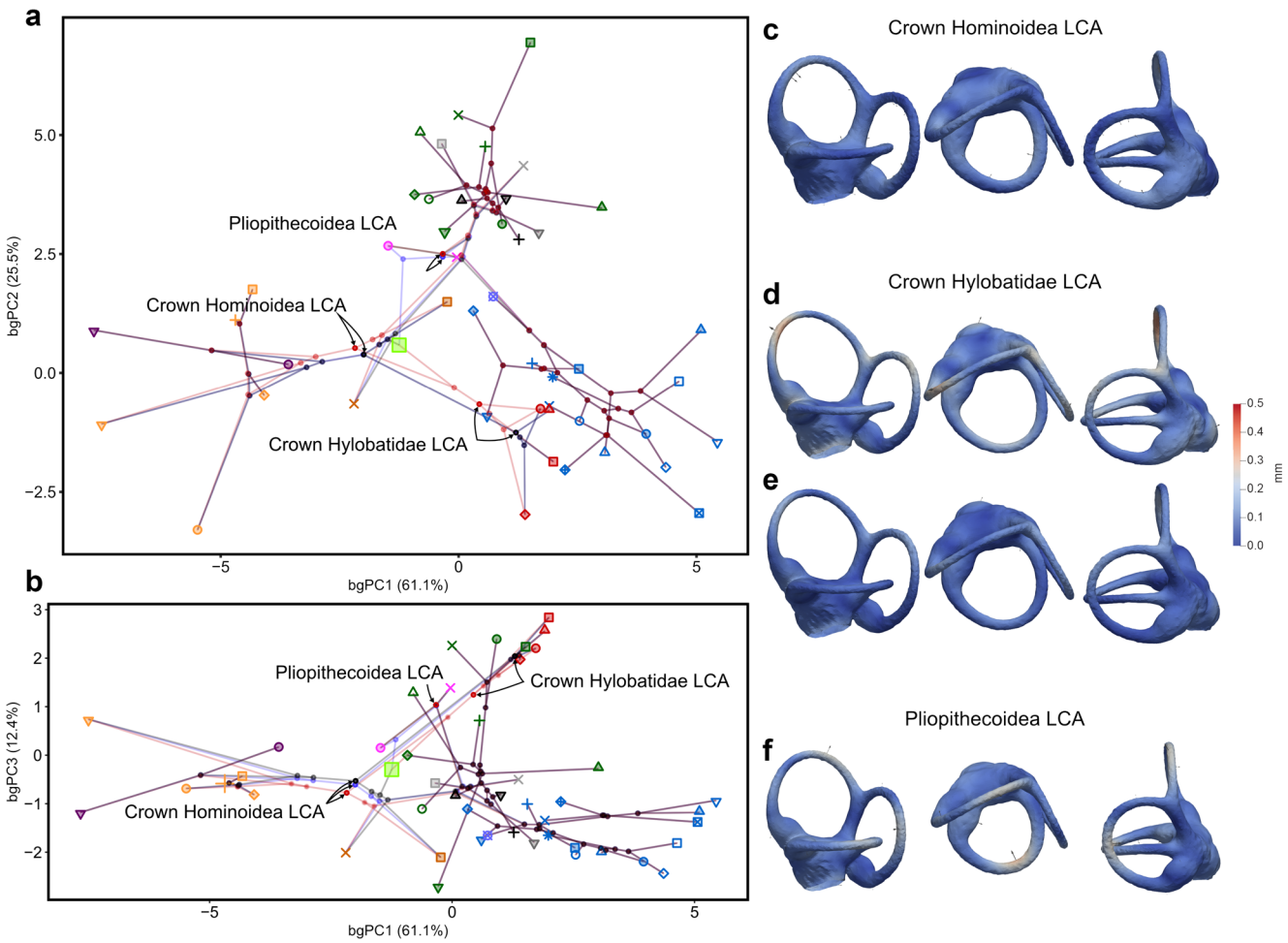

Fig. 3 **a**–**b**. Phylomorphospace based on the bgPC score genus averages obtained from the bgPCA shown in Fig. 2: bgPC2 vs. bgPC1 (**a**); bgPC3 vs. bgPC1 (**b**). The internal nodes and branches are colored based on the phylogenetic hypothesis used to estimate the LCA shape: pliopithecoid (stem catarrhine) hypothesis, blue; stem hylobatid hypothesis, red; nyanzapithecid (stem hominoid) hypothesis, black. Symbol colors are based on taxonomy as in Fig. 2. **c**–**f.** Shape estimates for the SCs and vestibule of selected LCAs in posterolateral (left), superolateral (middle), and posteromedial (right) views, were based on the nyanzapithecid (stem hominoid) hypothesis (**c**, **d**, **f**) and the stem hylobatid hypothesis (**e**). Results based on different phylogenetic hypotheses are provided in Online Resource 1: Figure S2. The 3D models are colored following a color gradient from blue (no displacement) to red (1.5 mm)

Table 3 Euclidean distances based on the bgPCA scores between *Oreopithecus bambolii* (both average and the two specimens separately) and the estimated last common ancestors (LCA) of crown hominoids, crown hylobatids, and pliopithecoids. The distances are given for the three phylogenetic tree topologies used for the phylomorphospace (Fig. 3; Online Resource 1: Fig. S3): tree 1, pliopithecoid stem catarrhine; tree 2, stem hylobatid; tree 3, nyanzapithecid stem hominoid. The shortest distance for each combination is in bold

	Crown hominoid LCA	Crown hylobatid LCA	Pliopithecoid LCA
Average (Tree 1)	**0.839**	3.814	2.449
Average (Tree 2)	**0.614**	3.822	2.507
Average (Tree 3)	**0.806**	3.822	2.507
Bac 62 (Tree 1)	**2.068**	2.538	3.449
Bac 62 (Tree 2)	**2.084**	2.547	3.513
Bac 62 (Tree 3)	**2.031**	2.547	3.513
Bac 183 (Tree 1)	**1.834**	5.130	2.080
Bac 183 (Tree 2)	**1.587**	5.136	2.106
Bac 183 (Tree 3)	**1.834**	5.136	2.106

Tooth morphology

Outer enamel surface and enamel-dentine junction shape

The cheek tooth measurements are provided in Table 4. The premolars (Fig. 1) display an oval (P3) to elliptical (P4) occlusal contour that is broader than long and has markedly rounded corners, although the P3 is more asymmetrical (mesiobuccally protruding). They show two tall, voluminous and inflated cusps that are joined by two (mesial and distal) crests. The mesial crest (hypoparacrista) is transversely aligned toward the protocone in the P3 and more mesially directed toward the preprotocrista in the P4. Together with the obliquely oriented preprotocrista and the shorter preparacrista, the hypoparacrista delimits a restricted mesial fovea. In both premolars (but more clearly in the P4) the thick postprotocrista appears to bifurcate along its course, with one end joining the distal marginal ridge and the other curving buccally to join the distal aspect of the paracone base; the latter distally encloses the talon basin, which is restricted (but less so than the mesial fovea). In contrast, a distinct postparacrista, shorter than the postprotocrista, can only be discerned in the P4, separating the buccal cingulum from the distal marginal ridge. The lingual cingulum is very wide in both premolars and extends from the mesial to the distal aspects of the crown until the ends of the preprotocrista and postprotocrista. The buccal cingulum is only similarly developed in the P4, whereas in the P3 it is thinner and distally continuous with the marginal ridge (Fig. 1). Both premolars have three roots, the two lingual ones being slenderer than the buccal.

The three molars (Fig. 1) display the same occlusal pattern and a similarly elongated and subrectangular occlusal contour that is much longer than broad. The M1 is the smallest molar and the M3 the largest (both in length and width), although differences are small and the proportions very similar, with the M1 being slightly narrower in relative terms than the other molars (Table 4). There are four tall and voluminous main cusps in a very median (non-peripheral) position on the occlusal surface, the lingual ones being located slightly more distally than the buccal cusps. The preprotocrista and the shorter preparacrista are obliquely oriented and converge on the mesial marginal ridge, while the more transversely oriented hypoparacrista joins the former at about its midway. Together, these three crests delimit a pit-like mesial fovea that is located toward the buccal half of the crown. A well-developed and centrally located protoconule (=paraconule) is present at the end of the preprotocrista on the mesial ridge (more clearly ascertainable in the M3 probably due to the lack of wear), lingually flanking the mesial fovea. There are no distinct crests linking the mesial and the distal cusps except for the well-developed crista obliqua, which displays a small but distinct (particularly, in the M2 and M3) metaconule (=centroconule) at about its midway, where the prehypocrista joins the crista obliqua. There are no distinct crests linking the distal cusps with the distal marginal ridge, but a poorly developed crest originates in distolingual direction from the metacone toward the hypocone, delimiting a small distal fovea from the rest of the talon basin. A small and centrally located hypoconule is present on the distal marginal ridge (more marked in M3 than in the other molars, probably due to wear). In the right M3, there is small but distinct secondary cuspule on the distolingual aspect of the protocone base, but a similar structure cannot be discerned on the other molars. The lingual cingulum is well developed and extends from the hypocone to the protoconule, progressively becoming wider (except at the base of the protocone, where it is very restricted or even interrupted) until becoming ledge-like at the mesiolingual corner of the crown. The buccal cingulum is more restricted and discontinuous (interrupted at the base of the two main cusps) but particularly well developed on the mesiobuccal aspect of the paracone and especially along most of the distal crown margin (but not surrounding the distal aspect of the hypocone).

The EDJ of the upper molars (Figs. 1 and 4a) shows the same pattern as the OES, except that some details are not well visible due to the moderate resolution of the scan. Nonetheless, the resolution is sufficient to detect the main features of the EDJ and to compare them with those of other Miocene specimens (Fig. 4). The EDJ morphology of Bac 62 M2 is consistent with that of MGUP TOS 001 (Fig. 4b; Sineo et al. 2024), with only minor differences, such as the less peripheral dentine horns, the more marked metaconule, and the hypoparacrista more transversely aligned toward the protocone in the latter. Their crest pattern may be summarized as follows: (a) obliquely oriented preprotocrista and preparacrista that merge on the mesial marginal ridge close to the centrally located protoconule, and transversely oriented hypoparacrista delimiting a pit-like and centrally located mesial fovea; (b) diagonally oriented crista obliqua that displays a centroconule at the junction of the

Table 4 Dental measurements (in mm) and proportions for the upper dentition of Bac 62. Side is given within parentheses

Tooth	MD	BL	BLm	BLd	BLI
P3 (right)	6.3	7.8			123.8
P4 (right)	6.1	8.0			131.1
M1 (right)	8.2	6.6	5.9	6.6	80.5
M1 (left)	8.4	6.7	6.1	6.7	79.8
M2 (right)	9.1	7.6	7.0	7.6	83.5
M2 (left)	9.4	8.0	6.8	8.0	85.1
M3 (right)	9.6	8.4	8.0	8.4	87.5
M3 (left)	9.7	8.3	7.3	8.3	85.6

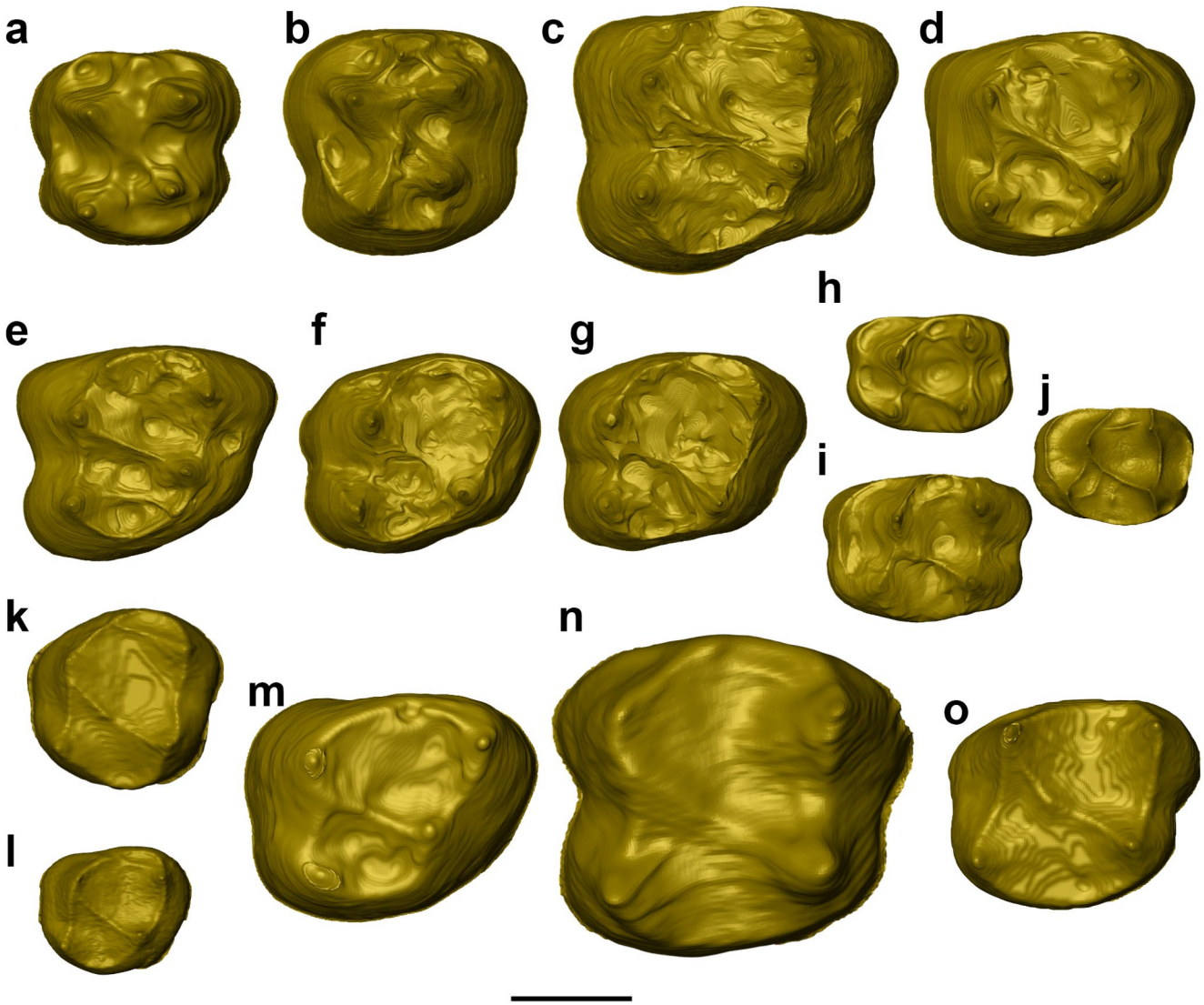

Fig. 4 Enamel-dentine junction of left M2s of selected hominoids and pliopithecoids, mesial toward the top: **a**. *Oreopithecus bambolii* (Bac 62); **b**. *Oreopithecus bambolii* (MGUP TOS 001); **c**. *Dryopithecus fontani* (IPS35026); **d**. *Pierolapithecus catalaunicus* (IPS21350); **e**. *Anoiapithecus brevirostris* (IPS43000); **f**. *Hispanopithecus crusafonti* (IPS1820); **g**. *Hispanopithecus laietanus* (IPS58339); **h**. *Barberapithecus huerzeleri* (IPS1724e); **i**. Anapithecinae indet. from Sant Quirze-Trinxera del Ferrocarril (MGSB48874); **j**. *Pliobates catalaoniae* (IPS94888); **k**. *Symphalangus syndactylus* (AMNH M-106583); **l**. *Hylobates muelleri* (MFN 7828); **m**. *Pongo pygmaeus* (MSNT) **n**. *Gorilla gorilla* (MCZ-20089); **o**. *Pan troglodytes* (AMNH-51204). Scale bar equals 5 mm

postprotocrista and hypometacrista, and obliquely oriented prehypocrista that joins the crista obliqua at about the level of the metaconule; (c) lack of postparacrista and premetacrista, and presence of a transverse crest that originates from the metacone and is directed toward the hypocone base or the prehypocrista.

Taken overall, this pattern is rather unique, as multiple of the aforementioned features differ from pliopithecoids, dryopithecines, and extant hominoids (namely, the centrally located protoconule, the pit-like mesial fovea, the obliquely oriented preparacrista, the metaconule, the prehypocrista directed toward the crista obliqua instead of the protocone, the lack of postparacrista and premetacrista). Furthermore, the molar EDJ of *Oreopithecus* displays a higher relief (both the dentine horns and crown walls), a more elongate occlusal contour (particularly compared with pliopithecoids, but also most hominoids, which further display a more asymmetric, subtrapezoidal contour), and less peripheral and more crowded dentine horns and crests (resulting in very restricted foveae on the central part of the crown). The presence of a transverse crest subdividing the talon basin is also frequent in dryopithecines, but in the latter it originates from the hypocone and is directed toward the metacone or postmetacrista, whereas in *Oreopithecus*

it originates from the metacone and is directed toward the hypocone or prehypocrista, which in turn is directed toward the crista obliqua, resulting in a very different occlusal pattern. Similarly, the well-developed cingula of *Oreopithecus* more closely resemble the well-developed cingula of pliopithecoids (which is the plesiomorphic condition for anthropoids) than the reduced cingula of dryopithecines and extant hominoids (which is derived), but *Oreopithecus* differs by the lack of a clear separation between the trigon basin and the buccal cingulum (due to the lack of crests linking the paracone and metacone). Coupled with the more obliquely oriented prehypocrista, this reflects the unique tendency of *Oreopithecus* to increase the peripheral 'basins' (at the EDJ level) at the expense of reducing the central ones. While there are no particular similarities between *Oreopithecus* and either dryopithecines or extant hominoids, the former resembles pliopithecoids in a couple of features: the more transverse orientation of the hypoparacrista (directed toward the preprotocrista rather than the protoconule); and the oblique orientation of the prehypocrista, which in pliopithecoids similarly joins the crista obliqua instead of the protocone, even though this is more marked in *Oreopithecus* and the straight course of its crista obliqua is more similar to that of hominoids than to that of pliopithecoids (where the postprotocrista originates more distally and progressively curves until merging with the hypometacrista). The lack of upper molar EDJ data precludes comparisons with nyanzapithecids.

Tooth tissue proportions

The results of tooth tissue proportions are summarized in Table 5. In terms of 3DAET, M1s tend to have lower values than M2s and M3s, and *Oreopithecus* is within the range of comparative samples of extinct and extant hominids. The molars of Bac 62 show relatively thin enamel in the M1s (3DRET = 12.9–15.4), and thicker enamel in the M2s (3DRET = 16.7–17.2) than in the M3s (3DRET = 15.9–16.5). This pattern is consistent with the variation observed in other catarrhine primates, even if hylobatids seem to exhibit the relatively thickest enamel in M3s (Table 5). The M2 values of Bac 62 are comparable to those of the *Oreopithecus* M2 MGUP TOS 001 (3DRET = 17.3). On average, for each molar position, *Oreopithecus* has thicker enamel than the dryopithecines and the extant hominoids, except for the M3s of hylobatids. In contrast, for 3DRED, *Oreopithecus* displays high values for all molar positions (8.5–9.3), which are within the range of dryopithecines, exceeding those of extant great apes, and are generally lower than in hylobatids. The comparison of 3DRED and 3DAET indices is shown in Fig. 5. Along the 3DAET axis, *Oreopithecus* is in the overlapping area between the dryopithecines (with generally smaller values) and the extant great apes (with higher values). In the 3DRED values, Bac 62 and MGUP TOS 001 exceed most of the comparative samples, except for one *Anoiapithecus* specimen in for the M1 (Fig. 5a), all specimens but a few hylobatids and *Anoiapithecus* in the M2 (Fig. 5b), whereas *Oreopithecus* M3s display a moderately high 3DRED, falling within the range of dryopithecines and below that of most hylobatids (Fig. 5c). The comparison of 3DRED and 3DAET indices thus indicates that *Oreopithecus* M1s and M2s have a thick enamel (as estimated by the former index) compared to their moderate tooth size (as attested by the latter index), but not the M3.

Discussion

New evidence from the Bac 62 partial cranium

Bony labyrinth

The new data obtained from the cranium Bac 62 helps in understanding the intraspecific variation of *O. bambolii*, while at the same time highlighting the uniqueness of this taxon and revealing conflicting phylogenetic signals even within a single anatomical system, as in the case of the vestibular system. The bony labyrinth of Bac 62 is broadly consistent with the previously studied (and roughly coeval) specimen, Bac 183 (Rook et al. 2004; Urciuoli et al. 2020, 2021b). However, it demonstrates a considerable amount of intraspecific variation in some features, particularly SC thickness (slenderer in Bac 62 than in Bac 183) and LSC proportions (relatively larger and broader in Bac 62). Although our results indicate that *Oreopithecus* displays a wider range of vestibular system shape variation than previously appreciated, the observed range variation does not exceed that of several other inspected species (especially when gorillas and orangutans are considered). As a result of this variation, Bac 62 shows closer affinities with hylobatids than Bac 183, although both specimens are remarkably close to hominids, consistent with a stem hominoid status with some superimposed convergences with the latter (Urciuoli et al. 2020, 2021b). Therefore, it would be preliminary to advocate the relaxation of predation selection pressures due to insularity for explaining the degree of variation displayed by the bony labyrinth of *Oreopithecus*—particularly given that the current morphofunctional understanding of the relationship between vestibular system bony labyrinth shape and function is still a matter of ongoing research.

Previous analyses of the inner ear bony labyrinth based on linear measurements inferred a limited locomotor agility for *Oreopithecus*, suggestive of slow, arboreal locomotion (Rook et al. 2004; Ryan et al. 2012)—slower than in

Table 5 Three-dimensional upper molar crown tissue proportion reported for *Oreopithecus bambolii* in this paper as compared with previously published results for both Miocene and extant hominoids. When the catalogue number is available, the side is given within parentheses next to it

Taxon	Catalog No.	V_e	V_{cdp}	SEDJ	3DAET	3DRET	3DRED	Reference
M1								
Oreopithecus bambolii	Bac 62 (L)	72.02	115.63	114.39	0.63	12.92	8.54	This study
Oreopithecus bambolii	Bac 62 (R)	83.09	111.42	111.80	0.74	15.44	9.07	This study
Anoiapithecus brevirostris	IPS43000 (L)	116.36	193.21	176.52	0.66	11.40	8.45	Fortuny et al. (2021)
Anoiapithecus brevirostris	IPS43000 (R)	128.92	184.37	180.82	0.71	12.53	8.86	Fortuny et al. (2021)
Pierolapithecus catalaunicus	IPS21350 (L)	122.50	173.19	166.02	0.74	13.24	8.92	Fortuny et al. (2021)
Hispanopithecus crusafonti	IPS1815 (L)	108.91	195.29	160.21	0.68	11.72	8.23	Fortuny et al. (2021)
Hispanopithecus crusafonti	IPS1818 (L)	166.05	234.26	188.77	0.88	14.27	8.92	Fortuny et al. (2021)
Hispanopithecus laietanus	IPS1844 (R)	139.92	198.82	169.53	0.83	14.14	8.91	Fortuny et al. (2021)
Pongo pygmaeus	—	188.01	333.33	203.89	0.92	13.3	8.26	Olejniczak et al. (2008)
Pongo pygmaeus	—	180.76	382.33	221.98	0.81	11.22	7.78	Olejniczak et al. (2008)
Pan troglodytes	—	114.84	293.06	173.19	0.66	9.98	7.31	Olejniczak et al. (2008)
M2								
Oreopithecus bambolii	Bac 62 (L)	115.97	147.77	127.74	0.91	17.17	9.22	This study
Oreopithecus bambolii	Bac 62 (R)	117.21	149.61	132.54	0.88	16.66	9.22	This study
Oreopithecus bambolii	MGUP TOS 001 (L)	143.39	178.79	147.22	0.97	17.29	9.29	Sineo et al. (2024)
Dryopithecus fontani	IPS35026 (L)	232.42	387.86	268.95	0.86	11.85	8.42	Fortuny et al. (2021)
Dryopithecus fontani	MGSB48486 (R)	150.92	279.89	220.85	0.68	10.45	8.13	Fortuny et al. (2021)
Anoiapithecus brevirostris	IPS35027 (R)	67.67	101.65	111.53	0.61	13.00	8.75	Fortuny et al. (2021)
Anoiapithecus brevirostris	IPS35027 (L)	116.07	163.47	150.56	0.77	14.10	8.92	Fortuny et al. (2021)
Anoiapithecus brevirostris	IPS43000 (R)	149.70	188.06	183.29	0.82	14.26	9.28	Fortuny et al. (2021)
Anoiapithecus brevirostris	IPS43000 (L)	146.35	246.50	198.92	0.74	11.73	8.42	Fortuny et al. (2021)
Pierolapithecus catalaunicus	IPS21350 (L)	187.55	247.58	199.93	0.94	14.94	9.12	Fortuny et al. (2021)
Pierolapithecus catalaunicus	IPS21350 (R)	185.54	255.77	188.19	0.99	15.53	9.00	Fortuny et al. (2021)
Hispanopithecus crusafonti	IPS1820 (L)	155.12	260.59	215.49	0.72	11.27	8.41	Fortuny et al. (2021)
Hispanopithecus laietanus	IPS1844	139.92	198.82	169.53	0.83	14.14	8.91	Fortuny et al. (2021)
Hispanopithecus laietanus	IPS58339 (L)	173.72	279.32	218.27	0.80	12.18	8.55	Fortuny et al. (2021)
Hylobates muelleri	MFN 7084	31.47	39.71	58.12	0.54	15.87	9.25	This study
Hylobates muelleri	MFN 7828	28.65	45.08	55.99	0.51	14.38	8.60	This study
Hylobates sp.	MFN 46511	41.85	50.82	65.89	0.64	17.15	9.37	This study
Symphalangus syndactylus	AMNH M-106583	70.31	106.11	97.74	0.72	15.19	8.72	This study
Pongo pygmaeus	—	201.55	289.89	202.22	1.00	15.06	8.87	Olejniczak et al. (2008)
Pongo pygmaeus	—	199.53	324.47	184.01	1.08	15.78	8.49	Olejniczak et al. (2008)
Pongo pygmaeus	—	196.42	330.50	202.01	0.97	14.06	8.40	Olejniczak et al. (2008)
Pongo pygmaeus	—	193.93	339.43	158.67	1.22	17.52	8.29	Olejniczak et al. (2008)
Pongo pygmaeus	—	271.74	500.61	307.12	0.88	11.14	8.16	Zanolli et al. (2019)
Pan troglodytes	—	147.19	310.31	171.63	0.86	12.67	7.81	Olejniczak et al. (2008)
M3								
Oreopithecus bambolii	Bac 62 (L)	112.38	152.47	132.48	0.85	15.88	9.03	This study
Oreopithecus bambolii	Bac 62 (R)	117.21	152.86	132.59	0.88	16.53	9.15	This study
Dryopithecus fontani	IPS35026 (L)	245.49	404.73	259.15	0.95	12.81	8.47	Fortuny et al. (2021)
Anoiapithecus brevirostris	IPS43000 (R)	146.15	206.70	183.10	0.80	13.50	8.92	Fortuny et al. (2021)
Pierolapithecus catalaunicus	IPS21350 (L)	128.13	136.55	137.16	0.93	18.14	9.78	Fortuny et al. (2021)
Hispanopithecus laietanus	IPS1772 (L)	89.07	122.33	115.59	0.77	15.52	8.99	Fortuny et al. (2021)
Hispanopithecus laietanus	IPS58340 (L)	156.95	255.38	205.12	0.77	12.06	8.52	Fortuny et al. (2021)
Hylobates muelleri	MFN 7814	30.31	30.61	47.04	0.64	20.60	9.97	This study
Hylobates muelleri	MFN 7828	18.17	24.91	38.61	0.47	16.12	9.00	This study
Hylobates sp.	MFN 7826 (L)	27.34	26.51	44.88	0.61	20.43	10.10	This study
Hylobates sp.	MFN 7826 (R)	27.70	30.18	44.88	0.62	19.83	9.72	This study
Symphalangus syndactylus	AMNH M-106583 (L)	48.58	56.99	65.40	0.74	19.30	9.48	This study
Symphalangus syndactylus	AMNH M-106583 (R)	48.50	54.68	63.78	0.76	20.03	9.61	This study
Gorilla gorilla	—	446.19	950.86	357.39	1.25	12.70	7.77	Olejniczak et al. (2008)
Pan troglodytes	—	126.9	221.13	180.79	0.7	11.61	8.30	Olejniczak et al. (2008)
Pan troglodytes	—	160.46	275	204.51	0.78	12.07	8.34	Olejniczak et al. (2008)
Pan troglodytes	—	176.83	304.38	191.97	0.92	13.69	8.34	Olejniczak et al. (2008)

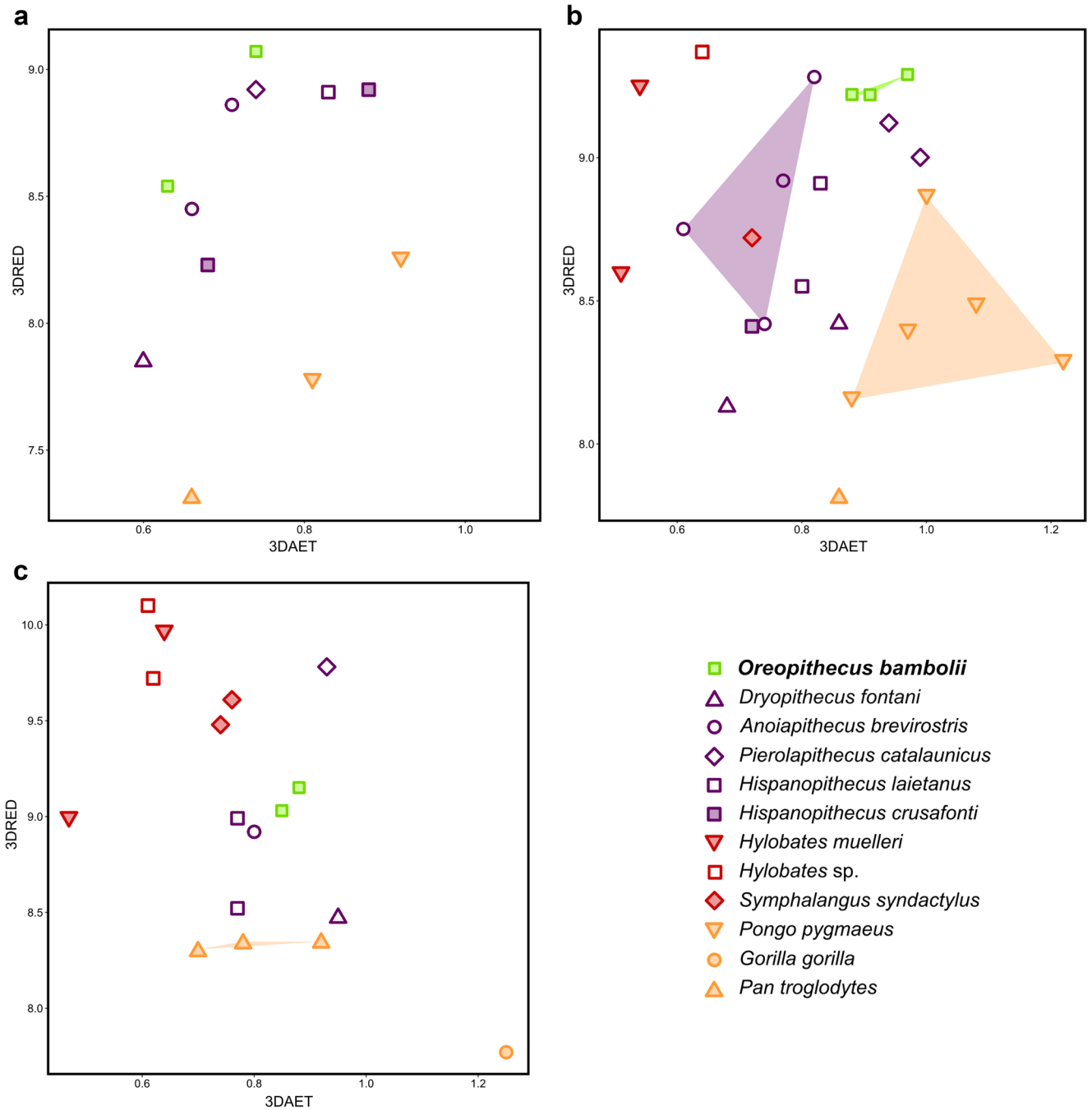

Fig. 5 Bivariate plots of 3DRET vs. 3DAET of *Oreopithecus* upper molars as compared with Miocene and extant hominoids: **a**. M1; **b**. M2; **c**. M3

proconsulids. This would be in agreement with the thick SCs, similar to those of hominids (Urciuoli et al. 2020), although other factors might be at play, such as allometry, as SC thickness has been shown to be correlated with SC and vestibule volume (Urciuoli et al. 2020, 2021a). Non-adaptive mechanisms, such as pleiotropy or genetic drift—as recently suggested for the remarkably thick SCs of Neandertals (Urciuoli et al. 2025)—cannot be discounted either, as the intraspecific variation here evidenced for *Oreopithecus* in SC thickness is at odds with the assumption that SC shape would have been under strong selection pressures. Furthermore, it has been shown that very similar SC shapes may reflect markedly different sensitivities to angular accelerations (David et al. 2022), so that a proper interpretation of SC function should rely on rigorous biophysical models for this structure (David et al. 2016) and possibly integrate the information from the

other vestibular structures involved in acceleration perception (namely, the macular organs; Smith et al. 2025).

From a phylogenetic viewpoint, Bac 62 also confirms the unique bony labyrinth morphology of *Oreopithecus*, previously suggested by Bac 183 and indicates that it combines features that align this taxon with different anthropoid clades (Urciuoli et al. 2021a, b). Specifically, the presence of a vertically compressed ASC, a very short CC, and a large vestibule relative to the SCs (synapomorphic with crown hominoids), coupled with the gibbon/orangutan-like morphology of the ASC, strongly support that *Oreopithecus* belongs to the ape and human clade (hominoids). However, these derived characteristics of crown hominoids are juxtaposed with the retention of a flat LSC, which is a symplesiomorphy of non-hominoid anthropoids and, thus, supports that *Oreopithecus* belongs to the hominoid stem lineage rather than the crown group. This is quantitatively supported by our multivariate analyses, which recover the two *Oreopithecus* specimens in a region of the morphospace outside the main clusters of extant anthropoid clades (Figs. 2 and 3), thus highlighting its morphological uniqueness.

Dental morphology

Our 3D analysis of dental tissue proportions confirms that *Oreopithecus* displays thick enamel, as previously shown both in 2D and 3D based on the lower molars (Zanolli et al. 2016). The enamel thickness displayed by *Oreopithecus* is not exceptionally high as compared with some extinct hominoids, even if generally higher than in extant great apes and dryopithecines (Fortuny et al. 2021), but further research is required in this sense regarding both nyanzapithecids and pliopithecoids. While it may hold taxonomic value in some cases, enamel thickness is not a reliable proxy for inferring phylogenetic relationships, not only due to its high intraspecific (metameric) variation but especially its high evolvability due to dietary selection pressures (Olejniczak et al. 2008; Zanolli et al. 2017).

The uniqueness of *Oreopithecus* is best reflected in its occlusal pattern. The upper cheek tooth morphology of Bac 62 is consistent with the previously described occlusal pattern for this taxon (Hürzeler 1949, 1958; Butler and Mills 1959; Szalay and Delson 1979; Harrison 1986, 1987; Harrison and Rook 1997; Alba et al. 2024; Sineo et al. 2024), despite some minor variations (such as the development of the metaconule and of the transverse crest originating from the hypocone). As noted by previous authors (Harrison 1986; Nengo et al. 2017, Pugh 2022; Alba et al. 2024; Pugh et al. 2025), the upper molar occlusal pattern of *Oreopithecus* is, in several features, most similar to that of nyanzapithecids generally (and especially *Nyanzapithecus*). Similarities include the elongate crown shape, the tall and inflated cusps, the prehypocrista directed toward the crista obliqua, and the pit-like and centrally located mesial fovea. However, it is noteworthy that the two latter features are not found together in most nyanzapithecid species (Alba et al. 2024), that some nyanzapithecid genera appear particularly plesiomorphic (especially, *Rangwapithecus*), and that *Oreopithecus* appears in contrast very autapomorphic. Similarities can also be found in the upper premolars (Kunimatsu et al. 2017), which coupled with similarities in the lower molars (Rossie and Cote 2022; Alba et al. 2024), support the close phylogenetic relationships between *Oreopithecus* and nyanzapithecids recovered by some cladistic analyses (Nengo et al. 2017).

As stressed in our comparisons above, one of the peculiarities of *Oreopithecus* is the apparent lack of mesiodistally oriented crests, not only the one linking the hypocone with the protocone (due to the obliquely oriented prehypocrista), but further those connecting the paracone and the metacone (i.e., postparacrista and premetacrista), which are similarly absent from (or poorly developed in) nyanzapithecids (e.g., Harrison 1986; Kunimatsu 1997; Nengo et al. 2017). Given the thick enamel of *Oreopithecus*, these crests might be simply poorly expressed at the OES and easily obliterated by wear. However, our inspection of the EDJ, coupled with previous results by Sineo et al. (2024), reveal that such crests are absent altogether. In this regard, it is thus unfortunate that the upper molar EDJ shape of any nyanzapithecid has been thus far reported, as it would help to clarify whether the similarities with *Oreopithecus* are homologous or homoplastic. In any case, our comparisons at both the OES and EDJ levels indicate that these features distinguish *Oreopithecus* from pliopithecoids, dryopithecines, and extant hominoids. Multiple features distinguish *Oreopithecus* from dryopithecines based on the upper molar occlusal pattern, both at the OES and EDJ levels (e.g., Fortuny et al. 2021), substantially weakening a possible link between them. The dental pattern of *Oreopithecus* is also different from that of pliopithecoids, although it displays some similarities. Besides the well-developed lingual cingulum (a plesiomorphic feature secondarily reduced in crown hominoids, and particularly great apes), the pliopithecoid condition more closely approaches that of *Oreopithecus* in the more obliquely oriented prehypocrista toward the crista obliqua and the more transverse hypoparacrista not directed toward the protoconule. Given that other similarities have been preliminarily reported for the lower molars at the EDJ level (Zanolli et al. 2022a), the aforementioned similarities in the upper molars deserve further investigation to clarify if they are just symplesiomorphies, as in the case of the lingual cingulum.

Phylogenetic implications

Taken together, the evidence from the vestibular system and the dental morphology reported here does not provide a clear answer to the phylogenetic uncertainties that still surround *Oreopithecus*—in part, due to the lack of available CT scans for the temporal bone and upper molars of nyanzapithecids, which preclude quantitatively evaluating the nyanzapithecid stem hominoid hypothesis (e.g., Harrison 1986; Nengo et al. 2017). Nevertheless, this is consistent with the stem hominoid signal obtained from the SC morphology (combining hominoid synapomorphies with more plesiomorphic features) as well as the external morphology of Bac 62 upper cheek teeth (see review in Alba et al. 2024). However, published evidence from the bony labyrinth of *Nyanzapithecus* (Nengo et al. 2017) indicates that this taxon already displays the derived LSC shape of crown hominoids, contrasting with the more plesiomorphic condition (flat LSC) of *Oreopithecus*. This weakens the possible hypothetical link with nyanzapithecids, suggesting either that *Oreopithecus* diverged before this feature evolved or that its LSC shape is a reversal. Similarly, the anterosuperior projecting anterior-most portion of the ASC displayed by *Oreopithecus*—found in hylobatids and orangutans (Urciuoli et al. 2021a, b) but absent from nyanzapithecids (Nengo et al. 2017) and other anthropoids—further weakens the presence of a direct link with nyanzapithecids.

The anterosuperior projecting ASC anterior-most portion of *Oreopithecus* might be used in support of the stem hylobatid hypothesis (Rütimeyer 1876), which is otherwise weakly supported by our analyses but would be consistent with closer postcranial similarities with hylobatids than great apes (Sarmiento 1987; Hammond et al. 2020). However, it is uncertain whether this feature is a crown hominoid synapomorphy subsequently reversed in hominines (i.e., a symplesiomorphy of hylobatids and orangutans) or an independently evolved features in hylobatids and orangutans (Urciuoli et al. 2021a, b). Only the second option would support (even if weakly) a possible link with hylobatids, whereas the first would also be consistent with a derived stem hominoid status for *Oreopithecus*. The lack of known petrosal bones for early crown hominoids hinders a more conclusive assessment of this character. The SC thickness of *Oreopithecus* does not appear particularly informative either. Even though the possession of thick canals is considered a hominid synapomorphy that contrasts with the thin and slender SCs, the larger-bodied siamangs display somewhat thicker SCs than gibbons, falling within the lower range of hominids and close to Bac 183 (Urciuoli et al. 2020, 2021b). Given the mild correlation between SC thickness and body size (Urciuoli et al. 2020, 2021a), the moderately thick (Bac 62) or thick (Bac183) SCs of *Oreopithecus* might be an allometric consequence of the great ape-like body mass of this taxon, but this would then apply irrespective of whether it evolved from the stem hylobatid stock or from a smaller-bodied stem hominoid. In any case, the upper molar occlusal pattern of hylobatids does not show any particular similarities with that of *Oreopithecus*, with the former more closely resembling that of hominids and most clearly displaying the opposite condition of spacious occlusal basins with very peripheral cusps.

Based on the analysis of the Bac 62 partial cranium, the pliopithecoid stem catarrhine hypothesis (Zanolli et al. 2022b) faces the greatest challenge, both from the vestibular system bony labyrinth and dental data. While the plesiomorphic flat LSC is consistent with a stem catarrhine status for *Oreopithecus*, this hypothesis would imply an independent evolution of all the crown-hominoid synapomorphies present in *Oreopithecus*—from the compressed ASC and short CC to the large vestibule—which as noted above are compatible with a stem hominoid status. These features are absent from the SCs and vestibule of the pliopithecoids *Epipliopithecus* and *Pliobates*, as well as in the other Oligocene stem catarrhines, supporting their stem catarrhine status, unlike in the case of *Oreopithecus* (Urciuoli et al. 2021a, 2022a). Similarly, the teeth of Bac 62 do not show clear affinities with pliopithecoids (Bouchet et al. 2024a) and rather present morphological features that suggest a link with basal hominoids in the external occlusal morphology (Harrison 1986, 1987, 1991; Rossie and Cote 2022; Alba et al. 2024). The pliopithecoid hypothesis, supported by preliminary results of the lower molar EDJ (Zanolli et al. 2022b) and previously noted structural similarities in their occlusal pattern (Hill et al. 2013; see review in Alba et al. 2024), does not receive much support from the upper molar EDJ either. The latter indicates a few closer similarities with pliopithecoids than with crown hominoids, but not to the extent that may be inferred from the OES of nyanzapithecid upper molars. Indeed, our results confirm that *Oreopithecus* lacks mesiodistal crests connecting the buccal cusps at the EDJ level, which differs from the pliopithecoid condition and reinforces instead the similarities with nyanzapithecids at the OES. It is uncertain whether the dental similarities between *Oreopithecus* and pliopithecoids are homologous or homoplastic, or whether in the first case they are just symplesiomorphic. However, they are not mutually excluding with those found with nyanzapithecids and thus require further research.

Conclusions

The analysis of the partial cranium Bac 62 provides new data on the internal cranial and dental morphology of *O. bambolii* but does not provide a clear answer about its phylogenetic relationships. The analysis of the inner ear bony labyrinth confirms previous results indicating that the SCs and vestibule of *Oreopithecus* are more derived than those of pliopithecoids and more consistent with a stem hominoid status, even if some features show closer resemblances with hominids or with hylobatids and orangutans. This is most consistent with the nyanzapithecid hypothesis, even if the latter is not particularly well supported based on the meager published data on the bony labyrinth of *Nyanzapithecus*. It is noteworthy that the new data on the SCs and vestibule of *Oreopithecus* reveal considerable intraspecific variation in some features, with the SCs of the newly reported specimen being slenderer and its LSC larger than in the previously reported specimen. This variability must not be necessarily interpreted in the context of insularity (as it can also be found in some extant taxa) but cautions against functional interpretations of SC thickness. The analysis of the OES and EDJ of the upper molars further contradicts the crown hominoid status of *Oreopithecus* and evinces somewhat greater similarities with pliopithecoids, while at the same time highlighting some differences that do not apply to nyanzapithecids (at least, at the OES level). All in all, the stem hominoid (and, in particular, nyanzapithecid) hypothesis remains the most plausible, although it is not exempt from problems and requires further confirmation by means of quantitative analyses of both the vestibular system bony labyrinth and the EDJ shape in a broad catarrhine context including pliopithecoids as well as members of other families of putative stem hominoids.

Supplementary Information The online version contains supplementary material available at https://doi.org/10.1007/s10914-025-09793-0.

Acknowledgements We dedicate this paper to Salvador Moyà-Solà, in recognition of his contributions to the study of the European fossil primate record, among many other taxa. Over the years, all of us collaborated with him more or less extensively, in some cases with a profound impact on our own research trajectories. This is especially true for three of us (A.U., F.B., and D.M.A.), who had the immense privilege of completing our doctoral studies under his supervision and would like to express our heartfelt thanks for his scientific guidance and mentorship throughout the years. Above all, he gave us the invaluable opportunity to follow our passion for paleontology, for which we will always be grateful. Finally, we extend our gratitude to Gabriel Aguirre Fernández and Jorge Carrillo Briceño for performing the microcomputed tomography scan of Bac 62 at the University of Zurich, as well as the LOEWE Centre for Translational Biodiversity Genomics (Frankfurt am Main, Germany) for letting us use the DeepFry cluster computer for computations.

Author contributions A.U. conceptualized the study; L.C. obtained the µCT scans of Bac 62; A.U. segmented the bony labyrinth data and C.Z. and F.B. segmented the dental material; A.U., C.Z., F.B., and J.A.M. performed the statistical analysis of the data; A.U., C.Z., and F.B. prepared the figures; A.U., C.Z., and D.M.A. wrote the manuscript with input from the remaining authors.

Funding Open Access funding provided thanks to the CRUE-CSIC agreement with Springer Nature. This publication is part of projects PID2024-159434NB-I00, PID2020-116908GB-I00, and PID2020-117289GB-I00, funded by the Agencia Estatal de Investigación of the Ministerio de Ciencia, Innovación y Universidades (MICIU/AEI/10.13039/501100011033) and ERDF, EU.Research has also been funded by the Generalitat de Catalunya/CERCA Programme and the Agència de Gestió d'Ajuts Universitaris i de Recerca of the Generalitat de Catalunya (Consolidated Research Groups 2022 SGR 00620 and 2022 SGR 01188).

Data availability All data generated during this study are included in this published article or in the supplementary information file, except for the 3D models, which can be accessed through the digital repository MorphoSource ([www.morphosource.com](https:/www.morphosource.com)). The models of the Bac 62 partial cranium and the semicircular canals and vestibule are openly available (at the following ark identifiers: [ark:/87602/m4/794093](https:/n2t.net/ark:/87602/m4/794093) and [ark:/87602/m4/794095](https:/n2t.net/ark:/87602/m4/794095)) whereas those from EDJ are currently embargoed due to ongoing research and only available upon request. The slice stack obtained from the µCT scan of Bac 62 is curated at the Naturhistorisches Museum Basel and can be accessed upon request.

Declarations

Conflict of interest The authors declare no competing interests.

References

Abbazzi L, Delfino M, Gallai G, Trebini L, Rook L (2008) New data on the vertebrate assemblage of Fiume Santo (North-West Sardinia, Italy), and overview on the Late Miocene Tusco-Sardinian Palaeobioprovince. Palaeontology 51:425–451. https://doi.org/10.1111/j.1475-4983.2008.00758.x

Alba DM (2010) Cognitive inferences in fossil apes (Primates: Hominoidea): does encephalization reflect intelligence? J Anthropol Sci 88:11–48.

Alba DM (2025). Research trajectory, works, and legacy of Salvador Moyà-Solà as a vertebrate paleobiologist. J Mamm Evol 32:24. https://doi.org/10.1007/s10914-025-09760-9

Alba DM, Moyà-Solà S, Köhler M (2001a) Canine reduction in the Miocene hominoid *Oreopithecus bambolii*: behavioural and evolutionary implications. J Hum Evol 40:1–16. https://doi.org/10.1006/jhev.2000.0439

Alba DM, Moyà-Solà S, Köhler M, Rook L (2001b) Heterochrony and the cranial anatomy of *Oreopithecus*: some cladistic fallacies and the significance of developmental constraints in phylogenetic analysis. In de Bonis L, Koufos GD, Andrews P (eds) Hominoid Evolution and Climatic Change in Europe, Vol. 2. Phylogeny of the Neogene Hominoid Primates of Eurasia. Cambridge University Press, Cambridge, pp 284–315. https://doi.org/10.1017/CBO9780511600449.013

Alba DM, Almécija S, DeMiguel D, Fortuny J, Pérez de los Ríos M, Pina M, Robles JM, Moyà-Solà S (2015) Miocene small-bodied ape from Eurasia sheds light on hominoid evolution. Science 350:aab2625. https://doi.org/10.1126/science.aab2625

Alba DM, Urciuoli A, Hammond AS, Almécija S, Rook L, Zanolli C (2024) Miocene ape evolution: Where does *Oreopithecus* fit in? Boll Soc Paleontol Ital 63:153–182. https://doi.org/10.4435/BSPI.2024.01

Almécija S, Shrewsbury M, Rook L, Moyà-Solà S (2014) The morphology of *Oreopithecus bambolii* pollical distal phalanx. Am J Phys Anthropol 153:582–597. https://doi.org/10.1002/ajpa.22458

Almécija S, Hammond AS, Thompson NE, Pugh KD, Moyà-Solà S, Alba DM (2021) Fossil apes and human evolution. Science 372:eabb4363. https://doi.org/10.1126/science.abb4363

Andrews P, Harrison T, Delson E, Bernor RL, Martin L (1996) Distribution and biochronology of European and Southwest Asian Miocene catarrhines. In: Bernor RL, Fahlbusch V, Mittmann H-W (eds) The Evolution of Western Eurasian Neogene Mammal Faunas. Columbia University Press, New York, pp 168–207

Beaudet A (2019) The inner ear of the *Paranthropus* specimen DNH 22 from Drimolen, South Africa. Am J Phys Anthropol 170:439–446. https://doi.org/10.1002/ajpa.23901

Beaudet A (2025) Investigating the primate fossil record using diffeomorphic deformation: what have we learnt? Bull Mem Soc Anthropol Paris 37:98–104. https://doi.org/10.4000/13pt4

Beaudet A, Dumoncel J, de Beer F, Duployer B, Durrleman S, Gilissen E, Hoffman J, Tenailleau C, Thackeray JF, Braga J (2016) Morphoarchitectural variation in South African fossil cercopithecoid endocasts. J Hum Evol 101:65–78. https://doi.org/10.1016/j.jhevol.2016.09.003

Begun DR, Kordos L (2004) Cranial evidence of the evolution of intelligence in fossil apes. In: Russon AE, Begun DR (eds) The Evolution of Thought. Evolutionary Origins of Great Ape Intelligence. Cambridge University Press, Cambridge, pp 260–279. https://doi.org/10.1017/CBO9780511542299.018

Benefit BR, McCrossin ML (2001) Craniodental comparisons of *Mabokopithecus* with *Oreopithecus* support an African origin of Oreopithecidae. Am J Phys Anthropol 114(S32):37–38

Bône A, Louis M, Martin B, Durrleman S (2018) Deformetrica 4: an open-source software for statistical shape analysis. In: Reuter M, Wachinger C, Lombaert H, Paniagua B, Lüthi M, Egger B (eds) Shape in Medical Imaging. Springer, Cham, pp 3–13. https://doi.org/10.1007/978-3-030-04747-4_1

Bouchet F, Zanolli C, Skinner MM, Urciuoli A, Fortuny J, Almécija S, Bernardini F, Tuniz C, Schillinger B, Moyà-Solà S, Alba DM (2024a) Molar enamel–dentine junction shape of *Pliobates cataloniae* and other Iberian pliopithecoids. J Hum Evol 195:103581. https://doi.org/10.1016/j.jhevol.2024.103581

Bouchet F, Zanolli C, Urciuoli A, Almécija S, Fortuny J, Robles JM, Beaudet A, Moyà-Solà S, Alba DM (2024b) The Miocene primate *Pliobates* is a pliopithecoid. Nat Commun 15:2822. https://doi.org/10.1038/s41467-024-47034-9

Bush EC, Simons EL, Allman JM (2004) High-resolution computed tomography study of the cranium of a fossil anthropoid primate, *Parapithecus grangeri*: New insights into the evolutionary history of primate sensory systems. Anat Rec 281A:1083–1087. https://doi.org/10.1002/ar.a.20113

Butler PM, Mills JRE (1959) A contribution to the odontology of *Oreopithecus*. Bull Brit Mus (Nat Hist) Geol 4:1–26

Cardini A, Polly PD (2020) Cross-validated between-group PCA scatterplots: a solution to spurious group separation? Evol Biol 47:85–95. https://doi.org/10.1007/s11692-020-09494-x

Casanovas-Vilar I, Alba DM, Garcés M, Robles JM, Moyà-Solà S (2011) Updated chronology for the Miocene hominoid radiation in Western Eurasia. Proc Natl Acad Sci USA 108:5554–5559. https://doi.org/10.1073/pnas.1018562108

David R, Stoessel A, Berthoz A, Spoor F, Bennequin D (2016) Assessing morphology and function of the semicircular duct system: introducing new in-situ visualization and software toolbox. Sci Rep 6:32772. https://doi.org/10.1038/srep32772

David R, Bronzati M, Benson RBJ (2022) Comment on "The early origin of a birdlike inner ear and the evolution of dinosaurian movement and vocalization". Science 376:eabl6710. https://doi.org/10.1126/science.abl6710

del Río J, Aristide L, dos Reis SF, Machado AC, Perez SI, Meloro C (2021) Allometry, function and shape diversification in the inner ear of platyrrhine primates. J Mamm Evol 28:135–143. https://doi.org/10.1007/s10914-019-09490-9

Delson E (1979) *Oreopithecus* is a cercopithecoid after all. Am J Phys Anthropol 50:431–432

Dumoncel J (2021) RToolsForDeformetrica. R package version 0.1. n. https://gitlab.com/jeandumoncel/tools-for-deformetrica/-/tree/master/src/R_script/RToolsForDeformetrica

Dumoncel J, Durrleman S, Braga J, Jessel JP, Subsol G (2014) Landmark-free 3D method for comparison of fossil hominins and hominids based on endocranium and EDJ shapes. Am J Phys Anthropol 153(S58):110

Durrleman S, Pennec X, Trouvé A, Ayache N, Braga J (2012a) Comparison of the endocranial ontogenies between chimpanzees and bonobos via temporal regression and spatiotemporal registration. J Hum Evol 62:74–88. https://doi.org/10.1016/j.jhevol.2011.10.004

Durrleman S, Prastawa M, Korenberg JR, Joshi S, Trouvé A, Gerig G (2012b) Topology preserving atlas construction from shape data without correspondence using sparse parameters. In: Ayache N, Delingette H, Golland P, Mori K (eds) Medical Image Computing and Computer Aided Intervention. Springer-Verlag, Berlin, pp 223–230. https://doi.org/10.1007/978-3-642-33454-2_28

Ekdale EG (2013) Comparative anatomy of the bony labyrinth (inner ear) of placental mammals. PLoS One 10:e0137149. https://doi.org/10.1371/journal.pone.0137149

Engesser B (2000) Gli studi di Johannes Hürzeler sull'*Oreopithecus* e storia del ritrovamento di "Sandrone". Atti Mus Stor Nat Maremma 18:7–23

Fortuny J, Zanolli C, Bernardini F, Tuniz C, Alba DM (2021) Dryopithecine palaeobiodiversity in the Iberian Miocene revisited on the basis of molar endostructural morphology. Palaeontology 64:531–554. https://doi.org/10.1111/pala.12540

Fulwood EL, Boyer DM, Kay RF (2016). Stem members of Platyrrhini are distinct from catarrhines in at least one derived cranial feature. J Hum Evol 100:16–24. https://doi.org/10.1016/j.jhevol.2016.08.001

Galbany J, Moyà-Solà S, Pérez-Pérez A (2006). Dental microwear variability on buccal tooth enamel surfaces of extant catarrhini and the Miocene fossil *Dryopithecus laietanus* (Hominoidea). Folia Primatol 76:325–341. https://doi.org/10.1159/000089531

Gervais P (1872a) Sur un singe fossile, d'un espèce non encore décrite, qui a été découvert au Monte Bamboli. C R Acad Sci Paris 74:1217–1223

Gervais P (1872b) Coup d'oeil sur les mammifères fossiles de l'Italie suivi de la description d'une espèce nouvelle de singes provenant des lignites du Monte Bamboli. J Zool 1:211–235

Gilbert CC, Ortiz A, Pugh KD, Campisano CJ, Patel BA, Singh NP, Fleagle JG, Patnaik R (2020) New Middle Miocene ape (Primates: Hylobatidae) from Ramnagar, India fills major gaps in the hominoid fossil record. Proc R Soc B 287:20201655. https://doi.org/10.1098/rspb.2020.1655

Glaunès JA, Joshi S (2006) Template estimation form unlabeled point set data and surfaces for computational anatomy. In: Pennec X (ed) Proceedings of the International Workshop on the Mathematical Foundations of Computational Anatomy Sophia-Antipolis. National Institute for Research in Digital Science and Technology (INRIA), Sophia-Antipolis, pp 28–39

Hammond AS, Rook L, Anaya AD, Cioppi E, Costeur L, Moyà-Solà S, Almécija S (2020) Insights into the lower torso in Late Miocene hominoid *Oreopithecus bambolii*. Proc Natl Acad Sci USA 117:278–284. https://doi.org/10.1073/pnas.1911896116

Harrison T (1986) New fossil anthropoids from the Middle Miocene of East Africa and their bearing on the origin of the Oreopithecidae. Am J Phys Anthropol 71:265–284. https://doi.org/10.1002/ajpa.1330710303

Harrison T (1987) A reassessment of the phylogenetic relationships of *Oreopithecus bambolii* Gervais. J Hum Evol 15:541–583. https://doi.org/10.1016/S0047-2484(86)80073-2

Harrison T (1989) New estimates of cranial capacity, body size and encephalization in *Oreopithecus bambolii*. Am J Phys Anthropol 78:237

Harrison T (1991) The implications of *Oreopithecus bambolii* for the origins of bipedalism. In: Senut B, Coppens Y (eds) Origine(s) de la Bipédie Chez les Hominidés. Editions du CNRS, Paris, pp 235–244

Harrison T, Rook L (1997) Enigmatic anthropoid or misunderstood ape? The phylogenetic status of *Oreopithecus bambolii* reconsidered. In: Begun DR, Ward CV, Rose MD (eds) Function, Phylogeny and Fossils: Miocene Hominoid Evolution and Adaptation. Plenum Press, New York, pp 327–362. https://doi.org/10.1007/978-1-4899-0075-3_16

Heffner RS (2004) Primate hearing from a mammalian perspective. Anat Rec A 281A:1111–1122. https://doi.org/10.1002/ar.a.20117

Hill A, Nengo IO, Rossie JB (2013) A *Rangwapithecus gordoni* mandible from the Early Miocene site of Songhor, Kenya. J Hum Evol 65:490–500. https://doi.org/10.1016/j.jhevol.2013.02.014

Hürzeler, J. (1949). Neubeschreibung von *Oreopithecus bambolii* Gervais. Schweiz Palaeontol Abh 66:1–20

Hürzeler J (1958) *Oreopithecus bambolii* Gervais. A preliminary report. Verh Naturforsch Ges Basel 69:1–48

Hussain R, Frater A, Calixto R, Karoui C, Margeta J, Wang Z, Hoen M, Delingette H, Patou F, Raffaelli C, Vandersteen C, Guevara N (2023). Anatomical variations of the human cochlea using imaging tool. J Clin Med 12:509. https://doi.org/10.3390/jcm12020509

Jungers WL (1987) Body size and morphometric affinities of the appendicular skeleton in *Oreopithecus bambolii* (IGF 11778). J Hum Evol 16:445–456. https://doi.org/10.1016/0047-2484(87)90072-8

Kay RF (2015). Biogeography in deep time – what do phylogenetics, geology, and paleoclimate tell us about early platyrrhine evolution? Mol Phylogenet Evol 82:358–374. https://doi.org/10.1016/j.ympev.2013.12.002

Kay RF, Fleagle JG, Mitchell TRT, Colbert M, Bown T, Powers DW (2008) The anatomy of *Dolichocebus gaimanensis*, a stem platyrrhine monkey from Argentina. J Hum Evol 54:323–382. https://doi.org/10.1016/j.jhevol.2007.09.002

Köhler M, Moyà-Solà S (1997) Ape-like or hominid-like? The positional behavior of *Oreopithecus bambolii* reconsidered. Proc Natl Acad Sci USA 94:11747–11750. https://doi.org/10.1073/pnas.94.21.11747

Köhler M, Moyà-Solà S (2003) Understanding the enigmatic ape *Oreopithecus bambolii*. Cour Forsch-Inst Senckenberg 243:111–123

Kuderna LFK, Gao H, Janiak MC, Kuhlwilm M, Orkin JD, Bataillon T, Manu S, Valenzuela A, Bergman J, Rousselle M, Silva FE, Agueda L, Blanc J, Gut M, de Vries D, Goodhead I, Harris RA, Raveendran M, Jensen A, Chuma IS, Horvath JE, Hvilsom C, Juan D, Frandsen P, Schraiber JG, de Melo FR, Bertuol F, Byrne H, Sampaio I, Farias I, Valsecchi J, Messias M, da Silva MNF, Trivedi M, Rossi R, Hrbek T, Andriaholinirina N, Rabarivola CJ, Zaramody A, Jolly CJ, Phillips-Conroy J, Wilkerson G, Abee C, Simmons JH, Fernandez-Duque E, Kanthaswamy S, Shiferaw F, Wu D, Zhou L, Shao Y, Zhang G, Keyyu JD, Knauf S, Le MD, Lizano E, Merker S, Navarro A, Nadler T, Khor CC, Lee J, Tan P, Lim WK, Kitchener AC, Zinner D, Gut I, Melin AD, Guschanski K, Schierup MH, Beck RMD, Umapathy G, Roos C, Boubli JP, Rogers J, Farh KK-H, Marques Bonet T (2023) A global catalog of whole-genome diversity from 233 primate species. Science 380:906–913. https://doi.org/10.1126/science.abn7829

Kunimatsu Y (1997) New species of *Nyanzapithecus* from Nachola, northern Kenya. Anthropol Sci 105:117–141.

Kunimatsu Y, Sawada Y, Sakai T, Saneyoshi M, Nakaya H, Yamamoto A, Nakatsukasa M (2017) The latest occurrence of the nyanzapithecines from the early Late Miocene Nakali Formation in Kenya, East Africa. Anthropol Sci 125:45–51.

Kunimatsu Y, Nakatsukas M, Shimizu D, Nakano Y, Ishida H (2019). Loss of the subarcuate fossa and the phylogeny of *Nacholapithecus*. J Hum Evol 131:22–27. https://doi.org/10.1016/j.jhevol.2019.03.004

Leakey LSB (1967) An Early Miocene member of Hominidae. Nature 213:155–163. https://doi.org/10.1038/213155a0

Leakey LSB (1968) Upper Miocene primates from Kenya. Nature 218:527–528. https://doi.org/10.1038/218527a0

Morimoto N, Kunimatsu Y, Nakatsukasa M, Ponce de León MS, Zollikofer CPE, Ishida H (2020) Variation of bony labyrinthine morphology in Mio-Plio-Pleistocene and modern anthropoids. Am J Phys Anthropol 173:680–700. https://doi.org/10.1002/ajpa.24098

Moyà-Solà S (2000) Viaje a los orígenes del bipedismo y una escala en la isla de los simios. In: Agustí J (ed), Antes de Lucy. El Agujero Negro de la Evolución Humana. Tusquets, Barcelona, pp 173–209

Moyà-Solà S, Köhler M (1996) A *Dryopithecus* skeleton and the origins of great-ape locomotion. Nature 379:156–159. https://doi.org/10.1038/379156a0

Moyà-Solà S, Köhler M (1997) The phylogenetic relationships of *Oreopithecus bambolii* Gervais, 1872. C R Acad Sci Paris 324:141–148

Moyà-Solà S, Köhler M (2000) Comprendere *Oreopithecus bambolii*, un ominoide fossile enigmatico. Atti Mus St Nat Maremma 18:39–65

Moyà-Solà S, Köhler M (2003) La evolución de *Oreopithecus bambolii* Gervais, 1872 (Primates, Anthropoidea) y la condición de insularidad. Col Paleontol Vol Extra 1:443–458

Moyà-Solà S, Köhler M, Rook L (1999) Evidence of hominid-like precision grip capability in the hand of the Miocene ape *Oreopithecus*. Proc Natl Acad Sci USA 96:313–317. https://doi.org/10.1073/pnas.96.1.313

Moyà-Solà S, Köhler M, Rook L (2005) The *Oreopithecus* thumb: a strange case in hominoid evolution. J Hum Evol 49:395–404. https://doi.org/10.1016/j.jhevol.2005.01.007

Nengo I, Tafforeau P, Gilbert CC, Fleagle JG, Miller ER, Feibel C, Fox DL, Feinberg J, Pugh KD, Berruyer C, Mana S, Engle Z, Spoor F (2017) New infant cranium from the African Miocene sheds light on ape evolution. Nature 548:169–174. https://doi.org/10.1038/nature23456

Oksanen J, Blanchet FG, Friendly M, Kindt R, Legendre P, McGlinn D, Minchin PR, O'Hara RB, Simpson GL, Solymos P, Stevens MHH, Szoecs E, Wagner H (2019) vegan: Community Ecology Package. R package version 2.5-6. https://CRAN.R-project.org/package=vegan

Olejniczak AJ, Tafforeau P, Feeney RNM, Martin LB (2008) Three-dimensional primate molar enamel thickness. J Hum Evol 54:187–195. https://doi.org/10.1016/j.jhevol.2007.09.014

Pan L, Dumoncel J, Mazurier A, Zanolli C (2020) Hominin diversity in East Asia during the Middle Pleistocene: A premolar endostructural perspective. J Hum Evol 148:102888. https://doi.org/10.1016/j.jhevol.2020.102888

Pugh KD (2022) Phylogenetic analysis of Middle-Late Miocene apes. J Hum Evol 165:103140. https://doi.org/10.1016/j.jhevol.2021.103140

Pugh KD, Strain JA, Gilbert CC (2025) Reanalysis of *Samburupithecus* reveals similarities to nyanzapithecines. J Hum Evol 200:103635. https://doi.org/10.1016/j.jhevol.2024.103635

R Core Team (2023) R: A language and environment for statistical computing. R Foundation for Statistical Computing, Vienna

Rabbitt RD (2019) Semicircular canal biomechanics in health and disease. J Neurophysiol 121:732–755. https://doi.org/10.1152/jn.00708.2018

Ramprashad F, Landolt J, Money K, Laufer J (1986). Comparative morphometric study of the vestibular system of the vertebrata: Reptilia, Aves, Amphibia, and Pisces. Acta Otolaryngol Supp 427:1–42

Revell LJ (2012) Phytools: an R package for phylogenetic comparative biology (and other things). Methods Ecol Evol 3:217–223. https://doi.org/10.1111/j.2041-210X.2011.00169.x

Rook L (2016) Geopalaeontological setting, chronology and palaeoenvironmental evolution of the Baccinello-Cinigiano Basin continental successions (Late Miocene, Italy). C R Palevol 15:825–836. https://doi.org/10.1016/j.crpv.2015.07.002

Rook L, Bondioli L, Köhler M, Moyà-Solà S, Macchiarelli R (1999) *Oreopithecus* was a bipedal ape after all: evidence from the iliac cancellous architecture. Proc Natl Acad Sci USA 96:8795–8799. https://doi.org/10.1073/pnas.96.15.8795

Rook L, Bondioli L, Casali F, Rossi M, Köhler M, Moyà-Solà S, Macchiarelli R (2004) The bony labyrinth of *Oreopithecus bambolii*. J Hum Evol 46:347–354. https://doi.org/10.1016/j.jhevol.2004.01.001

Rook L, Oms O, Benvenuti M, Papini M (2011) Magnetostratigraphy of the Late Miocene Baccinello–Cinigiano basin (Tuscany, Italy) and the age of *Oreopithecus bambolii* faunal assemblages. Palaeogeogr Palaeoclimatol Palaeoecol 305:286–294. https://doi.org/10.1016/j.palaeo.2011.03.010

Rossie JB, Cote SM (2022) Additional hominoid fossils from the early Miocene of the Lothidok Formation, Kenya. Am J Biol Anthropol 179:261–275. https://doi.org/10.1002/ajpa.24594

RStudio Team (2023) RStudio: Integrated Development for R. RStudio, Boston

Russo GA, Shapiro LJ (2013) Reevaluation of the lumbosacral region of *Oreopithecus bambolii*. J Hum Evol 65:253–265. https://doi.org/10.1016/j.jhevol.2013.05.004

Rütimeyer L (1876). Ueber Pliocen und Eisperiode auf beiden Seiten der Alpen. Universitaetsbuchdruckerei von C. Schultze, Basel

Ryan TM, Silcox MT, Walker A, Mao X, Begun DR, Benefit BR, Gingerich PD, Köhler M, Kordos L, McCrossin ML, Moyà-Solà S, Sanders WJ, Seiffert ER, Simons E, Zalmout IS, Spoor F (2012) Evolution of locomotion in Anthropoidea: the semicircular canal evidence. Proc R Soc B 279:3467–3475. https://doi.org/10.1098/rspb.2012.0939

Sarmiento EE (1987) The phylogenetic position of *Oreopithecus* and its significance in the origin of the Hominoidea. Am Mus Novit 2881:1–44

Schlager S (2017) Morpho and Rvcg—shape analysis in R: R-packages for geometric morphometrics, shape analysis and surface manipulations. In: Zheng G, Li S, Szekely G (eds) Statistical shape and deformation analysis. Academic Press, London, pp 217–256. https://doi.org/10.1016/B978-0-12-810493-4.00011-0

Schwalbe G (1915) Über den fossilen Affen *Oreopithecus bambolii*. Zugleich ein Beitrag zur Morphologie der Zähne der Primaten. Z Morphol Anthropol 19:149–254

Seiffert ER (2012) Early primate evolution in Afro-Arabia. Evol Anthropol 12:239–253. https://doi.org/10.1002/evan.21335

Shao Y, Zhou L, Li F, Zhao L, Zhang B-L, Shao F, Chen J-W, Chen C-Y, Bi X, Zhuang X-L, Zhu H-L, Hu J, Sun Z, Li X, Wang D, Rivas-González I, Wang S, Wang Y-M, Chen W, Li G, Lu H-M, Liu Y, Kuderna LFK, Farh KK-H, Fan P-F, Yu L, Li M, Liu Z-J, Tiley GP, Yoder AD, Roos C, Hayakawa T, Marques-Bonet T, Rogers J, Stenson PD, Cooper DN, Schierup MH, Yao Y-G, Zhang Y-P, Wang W, Qi X-G, Zhang G, Wu D-D (2023) Phylogenomic analyses provide insights into primate evolution. Science 380:913–924. https://doi.org/10.1126/science.abn6919

Sidlauskas B (2008) Continuous and arrested morphological diversification in sister clades of characiform fishes: a phylomorphospace approach. Evolution 62:3135–3156. https://doi.org/10.1111/j.1558-5646.2008.00519.x

Sievert C, Parmer C, Hocking T, Chamberlain S, Ram K, Corvellec M, Despouy P (2021) Plotly: Create interactive web graphics via plotly.js. R package version 4.10.0. https://plotly-r.com

Simons EL, Seiffert ER, Ryan TM, Attia Y (2007) A remarkable female cranium of the early Oligocene anthropoid *Aegyptopithecus zeuxis* (Catarrhini, Propliopithecidae). Proc Natl Acad Sci USA 104:8731–8736. https://doi.org/10.1073/pnas.0703129104

Sineo L, Zanolli C, Micciché RM, Santaluna G, Lauria G, Vita G, Di Patti C, Moggi Checchi J (2024) An *Oreopithecus bambolii* jaw in the Museum "Giorgio G. Gemmellaro" in Palermo. Boll Soc Paleontol Ital 63:137–143. https://doi.org/10.4435/BSPI.2024.07

Skinner MM, Gunz P, Wood BA, Hublin JJ (2008) Enamel-dentine junction (EDJ) morphology distinguishes the lower molars of *Australopithecus africanus* and *Paranthropus robustus*. J Hum Evol 55:979–988. https://doi.org/10.1016/j.jhevol.2007.09.012

Smith CM, Curhoys IS, Laitman JT (2023) First evidence of the link between internal and external structure of the human inner ear otolith system using 3D morphometric modeling. Sci Rep 13:4840. https://doi.org/10.1038/s41598-023-31235-1

Smith CM, Hammond AS, Urciuoli A, Braga J, Beaudet A, Cazenave M, Laitman JT, Almécija S (2025) Divergent otolithic systems in the inner ear of *Paranthropus robustus* and *Australopithecus africanus*. J Hum Evol 199:103624. https://doi.org/10.1016/j.jhevol.2024.103624

Susman RL (2004) *Oreopithecus bambolii*: an unlikely case of hominid-like grip capability in a Miocene ape. J Hum Evol 46:105–117. https://doi.org/10.1016/j.jhevol.2003.10.002

Susman RL (2005). *Oreopithecus*: still apelike after all these years. J Hum Evol 49:405–411. https://doi.org/10.1016/j.jhevol.2005.04.009

Szalay F, Delson E (1979) Evolutionary History of the Primates. Academic Press, New York

Urciuoli A, Alba DM (2023) Systematics of Miocene apes: State of the art of a neverending controversy. J Hum Evol 175:103309. https://doi.org/10.1016/j.jhevol.2022.103309

Urciuoli A, Zanolli C, Beaudet A, Dumoncel J, Santos F, Moya-Solà S, Alba DM (2020) The evolution of the vestibular apparatus in apes and humans. eLife 9:e51261. https://doi.org/10.7554/eLife.51261

Urciuoli A, Zanolli C, Beaudet A, Pina M, Almécija S, Moyà-Solà S, Alba DM (2021a) A comparative analysis of the vestibular apparatus in *Epipliopithecus vindobonensis*: Phylogenetic implications. J Hum Evol 151:102930. https://doi.org/10.1016/j.jhevol.2020.102930

Urciuoli A, Zanolli C, Almécija S, Beaudet A, Dumoncel J, Morimoto N, Nakatsukasa M, Moyà-Solà S, Begun DR, Alba DM (2021b) Reassessment of the phylogenetic relationships of the Late Miocene apes *Hispanopithecus* and *Rudapithecus* based on vestibular morphology. Proc Natl Acad Sci USA 118:e2015215118. https://doi.org/10.1073/pnas.2015215118

Urciuoli A, Zanolli C, Bouchet F, Almécija S, Moyà-Solà S, Alba DM (2022a) Semicircular canal morphology of the Miocene small-bodied catarrhine *Pliobates cataloniae*: phylogenetic implications. Am J Biol Anthropol 177(S73):187

Urciuoli A, Kubat J, Schisanowski L, Schrenk F, Zipfel B, Tawane M, Bam L, Alba DM, Kullmer O (2022b) Cochlear morphology of Indonesian *Homo erectus* from Sangiran. J Hum Evol 165:103163. https://doi.org/10.1016/j.jhevol.2022.103163

Urciuoli A, Martínez I, Quam R, Arsuaga JL, Keeling BA, Diez-Valero J, Conde-Valverde M (2025) Semicircular canals shed light on bottleneck events in the evolution of the Neanderthal clade. Nat Commun 16:972. https://doi.org/10.1038/s41467-025-56155-8

Yi Z, Liao W, Zanolli C, Wang W (2021) A robust alternative to assessing three-dimensional relative enamel thickness for the use in taxonomic assessment. Am J Phys Anthropol 174:555–567. https://doi.org/10.1002/ajpa.24187

Zalmout IS, Sanders WJ, MacLatchy L, Gunnell G, Al-Mufarreh YA, Ali MA, Nasser A-AH, Al-Masary AM, Al-Sobhi SA, Nadhra AO, Matari AH, Wilson JA, Gingerich PD (2010) New Oligocene primate from Saudi Arabia and the divergence of apes and Old World monkeys. Nature 466:360–364. https://doi.org/10.1038/nature09094

Zalmout IS, Sanders WJ, MacLatchy L, Gunnell G, Al-Mufarreh YA, Ali MA, Nasser A-AH, Al-Masary AM, Al-Sobhi SA, Nadhra AO, Matari AH, Wilson JA, Gingerich PD (2020) CT data of the partial cranium of SGS-UM 2009-002, *Saadanius hijazensis* (holotype). University of Michigan - Deep Blue Data. https://doi.org/10.7302/t0ty-pj64

Zanolli C, Dean C, Rook L, Bondioli L, Mazurier A, Macchiarelli R (2016) Enamel thickness and enamel growth in *Oreopithecus*: Combining microtomographic and histological evidence. C R Palevol 15:209–226. https://doi.org/10.1016/j.crpv.2015.02.001

Zanolli C, Bayle P, Bondioli L, Dean MC, Le Luyer M, Mazurier A, Morita W, Macchiarelli R (2017) Is the deciduous/permanent molar enamel thickness ratio a taxon-specific indicator in extant and extinct hominids? C R Palevol 16:702–714. https://doi.org/10.1016/j.crpv.2017.05.002

Zanolli C, Kullmer O, Kelley J, Bacon A-M, Demeter F, Dumoncel J, Fiorenza L, Grine FE, Hublin J-J, Nguyen AT, Nguyen TMH, Pan L, Schillinger B, Schrenk F, Skinner MM, Ji X, Macchiarelli R (2019) Evidence for increased hominid diversity in the Early to Middle Pleistocene of Indonesia. Nat Ecol Evol 3:755–764. https://doi.org/10.1038/s41559-019-0860-z

Zanolli C, Alba DM, Begun D, Bouchet F, Costeur L, Dean MC, Fortuny J, Kelley J, Le Cabec A, Morita W, Nakatsukasa M, Rook L, Urciuoli A (2022a) Tracking *Oreopithecus* evolutionary history: evidence from the enamel-dentine junction morphology. In: International Conference "*Oreopithecus*150. A Miocene Hominoid Enshrouded in a 150-Years-Long Mystery". Florence, Italy, pp 20–21.

Zanolli C, Urciuoli A, Delgado M, Davies TW, Bouchet F, Fortuny J, Beaudet A, Alba DM, Kullmer O, Skinner MM (2022b) The phylogenetic signal of the enamel-dentine junction of primate molars. Am J Phys Anthropol 177(S73):202–203

Zanolli C, Bouchet F, Fortuny J, Bernardini F, Tuniz C, Alba DM (2023) A reassessment of the distinctiveness of dryopithecine genera from the Iberian Miocene based on enamel-dentine junction geometric morphometric analyses. J Hum Evol 177:103326. https://doi.org/10.1016/j.jhevol.2023.103326

Zhang Y, Urciuoli A, Zanolli C, Kullmer O, Wu X (2024) Three-dimensional geometric morphometric analysis of the bony labyrinth of Xujiayao 6. J Hum Evol 189:103514. https://doi.org/10.1016/j.jhevol.2024.103514